R. & M. No. 3374

MINISTRY OF AVIATION

AERONAUTICAL RESEARCH COUNCIL
REPORTS AND MEMORANDA

A Direct Iteration Method for the Calculation of the Velocity Distribution of Bodies of Revolution and Symmetrical Profiles

By F. VANDREY

LONDON: HER MAJESTY'S STATIONERY OFFICE
1964
PRICE 15*s.* 0*d.* NET

A Direct Iteration Method for the Calculation of the Velocity Distribution of Bodies of Revolution and Symmetrical Profiles

By F. VANDREY

*Reports and Memoranda No. 3374**
August, 1951

Summary.

An integral equation is derived for the velocity on the surface of a given body of revolution or a given symmetrical profile in longitudinal flow, using the generation of a body by a vortex layer on its surface. The equation can be solved by the usual iteration method for linear integral equations of the second kind.

The method of generating a body by a vortex layer leads to formulae expressing the components of the velocity outside the body by means of its pressure distribution.

In general, the numerical work is greater for this method than for the indirect methods which use essentially a generation of the body by a distribution of sources and sinks on its axis. On the other hand, the method is not restricted to the case in which the analytic continuation of the flow into the interior of the body does not meet singularities outside the axis. The only requirement is that the shape of the body must have a continuous tangent, whereas its curvature may have isolated discontinuities.

Numerical examples are given for the two-dimensional case of a semi-infinite plate of constant thickness with a semi-circular leading edge, and for the three-dimensional case of a semi-infinite cylinder with three different heads (hemispherical, 2 caliber ogival and $\frac{1}{4}$ caliber rounded). The calculation is in good agreement with experimental results.

Some numerical tables are given in order to facilitate the calculation of the kernel of the integral equation which forms the major part of the numerical work.

1. *Introduction.*

The methods which have been developed by various authors (*see*, e.g. Ref. 1, 2) for the calculation of the velocity on the surface of a given body of revolution in a longitudinal flow, use essentially a generation of the body by a distribution of sources and sinks on its axis. First this generating distribution is determined (explicitly in Ref. 1, implicitly in Ref. 2) and then the induced velocities are obtained from its potential.

It is known that the generation of a body by a distribution of singularities on its axis requires the possibility of an analytic continuation of the flow into its interior without meeting any singularities outside the axis (Ref. 3, p. 141). In some cases of practical interest, e.g. if the body has a straight cylindrical central part or a rather blunt bow, this condition is not satisfied. The above mentioned methods will then fail on principle. Sometimes, they may nevertheless give a practically sufficient approximation, but it is rather difficult to estimate the degree of accuracy, and often the results of the calculation are obviously inadequate.

* Replaces A.R.L. Report No. ARL/R1/G/HY/12/2—A.R.C. 14 579.

These difficulties can only be overcome by distributing the generating singularities on the surface of the body instead of on its axis. An obvious generalisation of the methods[1, 2] would be the use of a distribution of source rings on the surface of the body. This will in fact give the solution of the problem in almost any case of practical interest, the requirement here being only that the shape of the body has a continuous tangent.

The amount of numerical work involved in the solution for a particular body will of course be much greater for this method than for the methods of Refs. 1 and 2, due to the facts that a source ring is a much more complicated mathematical object than a point source and that the singularities are situated on a curved surface instead of on a straight line.

A reduction of the numerical work can however be achieved by making a direct approach to the required velocity distribution without a previous determination of a generating distribution of source rings. This will be done in the present report.

Instead of supposing the body to be generated by source rings, it will be supposed to be generated by a vortex layer on its surface (*see*, e.g. Ref. 4, p. 10). The circulation of these vortices per unit length of arc of the shape gives directly the required velocity at the surface of the body (with a negative sign).

In the case of the indirect method referred to in paragraphs 3 and 4 above, the generating source distribution can be obtained from an integral equation of the second kind which expresses the condition of zero normal velocity at the surface of the body. An application of the same idea to the case of a generating vortex layer would lead to an integral equation of the first kind. These equations present considerable mathematical difficulties and cannot be solved by the relatively simple method of iteration.

An integral equation of the second kind for the generating vortex layer can, however, be obtained from the requirement that it must compensate the external parallel flow to zero in the interior of the body. This equation can be solved by iteration.

The method of generating a body by a vortex layer on its surface requires for its application only that the shape of the body should have a continuous tangent, whereas its curvature may have isolated discontinuities.

This method is not restricted to bodies of revolution, but is equally suitable for a two-dimensional body with an axis of symmetry, i.e. a symmetrical profile. In this case, the vortex layer consists of pairs of vortices of opposite circulation instead of vortex rings. Both cases of a body of revolution and a symmetrical profile will therefore be considered simultaneously in the following.

From the practical point of view, the method of vortex layers will, however, be restricted to cases where the indirect methods are bound or at least likely to fail, as the numerical work involved is in general greater here.

2. *The Boundary Problem for the Determination of the Velocity on the Surface of a Symmetrical Body in Longitudinal Flow.*

(a) The following general consideration holds for a body of revolution as well as for a symmetrical profile.

The shape of the body will be supposed to be a continuous curve, joining two points of the axis of symmetry at a distance L from each other. L may be infinite, in this case the diameter of the body may have a finite limit $\neq 0$. The tangent of the shape will be supposed to be continuous, but its curvature may have isolated discontinuities.

Let x denote the co-ordinate in the direction of the axis ($x = 0$ at the bow of the body), y the co-ordinate perpendicular to the axis. Let the shape of the body be given by

$$x = x(s);\ y = y(s), \tag{1}$$

s being its length of arc ($s = 0$ at the bow, $s = S$ at the stern). Then

$$\left.\begin{aligned} & x(0) = y(0) = 0 \\ \text{and} \quad & x(S) = L;\ y(S) = 0 \text{ for a finite body} \\ \text{or} \quad & x(\infty) = \infty;\ y(\infty) = Y \text{ for a semi-infinite body,} \end{aligned}\right\} \tag{2}$$

respectively.

In the case when the elimination of s from (1) gives a univalued function $y(x)$, preference will be given to the representation of the shape by

$$\left.\begin{aligned} & y = y(x) \\ \text{with} \quad & y(0) = y(L) = 0 \\ \text{or} \quad & y(0) = 0,\ y(\infty) = Y. \end{aligned}\right\} \tag{3}$$

(b) The surface Σ of the body divides the whole (two- or three-dimensional) space into two regions R_{ext} outside and R_{int} inside the body. Assume now both regions R_{ext} and R_{int} to be occupied by the fluid. Let the fluid in R_{ext} move past the body with a velocity V (in the direction of $+ x$), and *let the fluid in* R_{int} *be at rest* (Fig. 1).

The whole space $R_{ext} + R_{int}$ can then be regarded as a single region of flow in which Σ is a surface of discontinuity of the velocity. The normal component of the velocity being, however, continuous ($= 0$) on Σ the remaining discontinuity of the tangential component can be produced by a *vortex layer on the surface of the body.*

Let $w(s)$ be the velocity at the point s of Σ. The circulation of an element ds of Σ will then be

$$d\Gamma(s) = -\operatorname{sgn} y\ w(s)\ ds, \tag{4}$$

i.e. the vortex layer will consist of vortex rings of the strength $-w(s)$ per unit length of arc in the case of a body of revolution, and of pairs of vortices with equal strength and opposite sign in the case of a symmetrical profile (Fig. 2).

(c) *Let now a velocity* $-V$ *in the direction of* x *be superposed to the whole flow*, so that the fluid in R_{ext} is at rest at infinity. There will then be a uniform parallel flow of velocity $-V$ in R_{int}, where the fluid was at rest before. The potential Φ_{int} of this flow will be

$$\Phi_{int} = -Vx. \tag{5}$$

This flow is produced by the vortex layer on the surface Σ. The problem of determinating the velocity $w(s)$ on Σ is therefore equivalent to the following problem:

'A distribution of vortices (rings or pairs) is to be determined on the surface Σ of the body which produces a uniform parallel flow of potential $\Phi_{int} = -Vx$ in the region R_{int} inside Σ'.

The circulation of this vortex layer per unit length of arc gives the required velocity distribution on Σ. The pressure distribution can then be obtained from Bernoulli's equation.

3. *Derivation of an Integral Equation for the Velocity on the Surface.*

The boundary problem of the preceding section leads to a linear integral equation of the second kind for the velocity. This equation will be derived in the following section, again simultaneously for the two-dimensional and for the three-dimensional case.

Let $P_1 = (s) = (x, y)$ and $P_2 = (s+ds) = (x+dx, y+dy)$ be two points of the surface Σ close to each other (Fig. 3). If the vortex layer on Σ produces a uniform parallel flow of velocity $-V$ inside Σ the difference of the potential at P_1 and P_2 along the inner side of the element of arc ds will be

$$d\Phi_{\text{int}} = -V\,dx. \tag{6}$$

This difference is produced by

(1) the vortices on the part $P_1 P_2$ of Σ

(2) the vortices on Σ outside $P_1 P_2$

$$d\Phi_{\text{int}} = \phi_1 + \phi_2. \tag{7}$$

The contribution of the vortices on $P_1 P_2$ equals half of their circulation {cf. (4)}

$$\phi_1 = -\tfrac{1}{2} w(s)\,ds. \tag{8}$$

The contribution of the vortices on Σ outside $P_1 P_2$ is obtained by an integration. Let

$$\left.\begin{aligned} u(s,\sigma) &= -\frac{w(\sigma)d\sigma}{2\pi\eta(\sigma)}\,u^*(s,\sigma) \\ v(s,\sigma) &= -\frac{w(\sigma)d\sigma}{2\pi\eta(\sigma)}\,v^*(s,\sigma) \end{aligned}\right\} \tag{9}$$

be the components of the velocity which a vortex (ring or pair) of strength $-w(\sigma)d\sigma$, situated at the variable point (σ) of the surface {co-ordinates $\xi(\sigma)$, $\eta(\sigma)$}, induces at the pivotal point $(s) = \{x(s), y(s)\}$. This vortex will then produce the difference of the potential between P_1 and P_2

$$d\phi_2 = -\frac{w(\sigma)d\sigma}{2\pi\eta(\sigma)}\{u^*(s,\sigma)dx + v^*(s,\sigma)dy\}. \tag{10}$$

All the vortices on Σ will therefore produce the difference of the potential

$$\begin{aligned} d\Phi_{\text{int}} &= \phi_1 + \int_{\sigma=0}^{S} d\phi_2 \\ &= -\tfrac{1}{2}w(s)ds - \frac{1}{2\pi}\int_0^S w(\sigma)\frac{u^*dx + v^*dy}{\eta}\,d\sigma. \end{aligned} \tag{11}$$

From (6) and (11), the equation for $w(s)$ is as follows:

$$-Vdx = -\tfrac{1}{2}w(s)ds - \frac{1}{2\pi}\int_0^S w(\sigma)\frac{u^*dx + v^*dy}{\eta}\,d\sigma. \tag{12}$$

Dividing by $\frac{1}{2}\,Vds$ and introducing the non-dimensional velocity

$$w^*(s) = \frac{w(s)}{V}, \tag{13}$$

(12) is reduced to the final form

$$w^*(s) = 2\frac{dx}{ds} - \frac{1}{\pi}\int_0^S w^*(\sigma)\frac{u^*(s,\sigma)\dfrac{dx}{ds} + v^*(s,\sigma)\dfrac{dy}{ds}}{\eta(\sigma)}\,d\sigma \tag{14}$$

of a linear integral equation of the second kind for the velocity.

In the practically most important case in which the shape of the body can be represented by a univalued function $y = y(x)$ {cf. (3)}, (14) can still be somewhat simplified. (14) is multiplied by

$$\frac{ds}{dx} = \sqrt{(1+y'^2)}. \tag{15}$$

The introduction of the strength of the vortex layer per unit length of the axis

$$\gamma^* = w^*\sqrt{(1+y'^2)} \tag{16}$$

gives then the result

$$\gamma^*(x) = 2 - \frac{1}{\pi}\int_0^L \gamma^*(\xi)\,\frac{u^* + y'v^*}{\eta}\,d\xi. \tag{17}$$

If γ^* has been determined from this equation, (16) gives immediately the velocity

$$w^*(x) = \frac{\gamma^*(x)}{\sqrt{(1+y'^2)}}. \tag{18}$$

The non-dimensional velocity components u^*, v^* in the kernel of the integral equations (14) and (17) are in the two-dimensional case of a symmetrical profile

$$\left.\begin{aligned} u^* &= \left\{\frac{\frac{y}{\eta}-1}{\left(\frac{x-\xi}{\eta}\right)^2+\left(\frac{y}{\eta}-1\right)^2} - \frac{\frac{y}{\eta}+1}{\left(\frac{x-\xi}{\eta}\right)^2+\left(\frac{y}{\eta}+1\right)^2}\right\} \\ v^* &= \frac{x-\xi}{\eta}\left\{\frac{1}{\left(\frac{x-\xi}{\eta}\right)^2+\left(\frac{y}{\eta}-1\right)^2} - \frac{1}{\left(\frac{x-\xi}{\eta}\right)^2+\left(\frac{y}{\eta}+1\right)^2}\right\}. \end{aligned}\right\} \tag{19}$$

These expressions can easily be derived from the potential of a pair of vortices of circulation $\pm\Gamma$ situated at the points $\xi_1 \pm \eta$.

$$\Phi = \frac{\Gamma}{2\pi}\left(\tan^{-1}\frac{y-\eta}{x-\xi} - \tan^{-1}\frac{y+\eta}{x-\xi}\right). \tag{20}$$

In the three-dimensional case of a body of revolution, u^* and v^* are

$$\left.\begin{aligned} u^* &= \frac{1}{\sqrt{\left\{\left(\frac{x-\xi}{\eta}\right)^2+\left(\frac{y}{\eta}+1\right)^2\right\}}}\left[K(k) - \left\{1 + \frac{2\left(\frac{y}{\eta}-1\right)}{\left(\frac{x-\xi}{\eta}\right)^2+\left(\frac{y}{\eta}-1\right)^2}\right\}E(k)\right] \\ v^* &= \frac{-\frac{x-\xi}{\eta}}{\frac{y}{\eta}\sqrt{\left\{\left(\frac{x-\xi}{\eta}\right)^2+\left(\frac{y}{\eta}+1\right)^2\right\}}}\left[K(k) - \left\{1 + \frac{2\frac{y}{\eta}}{\left(\frac{x-\xi}{\eta}\right)^2+\left(\frac{y}{\eta}-1\right)^2}\right\}E(k)\right] \end{aligned}\right\} \tag{21}$$

with

$$\left.\begin{aligned} k^2 &= \frac{4\frac{y}{\eta}}{\left(\frac{x-\xi}{\eta}\right)^2+\left(\frac{y}{\eta}+1\right)^2} \\ K(k) &= \int_0^{\pi/2}\frac{d\psi}{\sqrt{(1-k^2\sin^2\psi)}}\,;\; E(k) = \int_0^{\pi/2}\sqrt{(1-k^2\sin^2\psi)}\,d\psi. \end{aligned}\right\} \tag{21a}$$

These expressions can be derived, for example, from the stream function of a vortex ring (Ref. 5 paragraph 161). Tables of u^* and v^* for the vortex ring have been computed by Küchemann (Ref. 6).

4. *Discussion of the Integral Equation.*

For simplicity, the following discussion will be restricted to the most important case that the body is finite and that its shape can be represented by a univalued function $y(x)$, i.e. to the form (17), (18) of the integral equation for the velocity. The extension of the more general cases is not difficult and gives essentially the same result.

The two-dimensional and the three-dimensional case will be treated separately, as far as the kernel of (17) is concerned. The iteration method for the solution will, however, be discussed simultaneously for both cases.

4.1. *Two-Dimensional Case.*

In the discussion of the kernel of (17)

$$K(x, \xi) = \frac{u^* + y'v^*}{\eta}, \tag{22}$$

i.e. with respect to (19)

$$K(x, \xi) = \frac{(y+\eta) - y'(x-\xi)}{(x-\xi)^2 + (y+\eta)^2} - \frac{(y-\eta) - y'(x-\xi)}{(x-\xi)^2 + (y-\eta)^2} \tag{23}$$

$$K(x, \xi) = \frac{2\eta\,\{(x-\xi)^2 + (\eta^2 - y^2) + 2yy'(x-\xi)\}}{\{(x-\xi)^2 + (y+\eta)^2\}\,\{(x-\xi)^2 + (y-\eta)^2\}}, \tag{24}$$

in the two-dimensional case, special attention has only to be paid to the cases

$$\xi = 0,\ \xi = L,\ \xi = x$$

and to the combined cases

$$\xi = x = 0 \text{ and } \xi = x = L,$$

where singularities may be expected.

Consider first the case $x \neq 0$ and $x \neq L$. The introduction of $\xi = 0$, $\eta = 0$ and $\xi = L$, $\eta = 0$ into (24) gives then immediately the result

$$K(x, 0) = K(x, L) = 0. \tag{25}$$

The case $\xi = x$ has to be treated by means of a development in series. For sufficiently small values of $(x-\xi)$, η will be

$$\eta \approx y - (x-\xi)y' + \tfrac{1}{2}(x-\xi)^2 y''. \tag{26}$$

The introduction of (26) into (24) gives the result

$$K(x, x) = \tfrac{1}{2}\left(\frac{1}{y} + \frac{y''}{1+y'^2}\right). \tag{27}$$

$K(x, \xi)$ is therefore finite at $\xi = x$ in the case $x \neq 0$ and $x \neq L$. As $y(x)$ and $y'(x)$ are supposed to be continuous in $0 < x < L$, $K(x, \xi)$ has a discontinuity at $\xi = x$ only, if $y''(x)$ is discontinuous, i.e. at the points where the curvature of the shape is discontinuous.

Consider now the cases $x = 0$ or $x = L$, $y = 0$. In order to cover the cases of practical interest, suppose further that

$$y \approx a\sqrt{x} \qquad \text{for } x \approx 0 \tag{28}$$

$$y \approx b(L-x) \text{ for } x \approx L,\ b > 0\,. \tag{29}$$

First

$$K(0, \xi) = \lim_{x \to 0} K(x, \xi) \text{ and } K(L, \xi) = \lim_{x \to L} K(x, \xi) \tag{30}$$

have to be determined.

$K(0, \xi)$ is obtained by the introduction of

$$x = 0, y = 0, \lim_{x \to 0} 2yy' = a^2 \tag{31}$$

into (24):

$$K(0, \xi) = \frac{2\eta(\xi^2 + \eta^2 - a^2\xi)}{(\xi^2 + \eta^2)^2} \tag{32}$$

Now let $\xi \to 0$. Then $K(0, 0)$ will be with respect to $\eta \approx a\sqrt{\xi}$

$$K(0, 0) = \lim_{\xi \to 0} \frac{2a(\xi^2 + a^2\xi - a^2\xi)\sqrt{\xi}}{(\xi^2 + a^2\xi)^2} = 0\,. \tag{33}$$

$K(L, \xi)$ is obtained correspondingly by introducing

$$x = L, y = 0, \lim_{x \to L} 2yy' = 0 \tag{34}$$

into (24).

$$K(L, \xi) = \frac{2\eta}{(L-\xi)^2 + \eta^2}\,. \tag{35}$$

Now let $\xi \to L$. Then $K(L, \xi)$ will be with respect to $\eta \to b(L-\xi)$

$$K(L, \xi) \to \frac{2b}{1 + b^2} \frac{1}{L - \xi} \to \infty\,. \tag{36}$$

The integral

$$T = \int_0^L \gamma^*(\xi) K(L, \xi) d\xi \tag{37}$$

will, however, be finite, as the velocity $w(x)$ and therefore

$$\gamma^*(x) = \frac{w(x)}{V} \sqrt{(1 + y'^2)} \tag{38}$$

tends to zero for $x \to l$, where the flow past the symmetrical profile has a stagnation point.

4.2. *Three-Dimensional Case.*

The discussion of $K(x, \xi)$ in the three-dimensional case follows the same general line as in two dimensions. With respect to (21), ($K(x, \xi)$ will be

$$K(x, \xi) = \frac{u^* + y'v^*}{\eta}$$

$$= \frac{1}{\sqrt{\{(x-\xi)^2 + (y+\eta)^2\}}} \left[K(k) - \left\{ 1 + \frac{2\eta(y-\eta)}{(x-\xi)^2 + (y-\eta)^2} \right\} E(k) - \right.$$

$$\left. - \frac{y'}{y} (x-\xi) \left\{ K(k) - \left(1 + \frac{2\eta y}{(x-\xi)^2 + (y-\eta)^2} \right) E(k) \right\} \right] \tag{39}$$

with

$$k^2 = \frac{4y\eta}{(x-\xi)^2 + (y+\eta)^2} \tag{39a}$$

or

$$K(x, \xi) = \frac{1}{\sqrt{\{(x-\xi)^2 + (y+\eta)^2\}}} \left[\left\{ 1 - \frac{y'}{y} (x-\xi) \right\} \left\{ K(k) - E(k) \right\} - \right.$$

$$\left. - \frac{2\eta[y - \eta - y'(x-\xi)]}{(x-\xi)^2 + (y-\eta)^2} E(k) \right]. \tag{40}$$

Consider first the case $x \neq 0$, $x \neq L$. The introduction of $\xi = 0$, $\eta = 0$ or $\xi = L$, $\eta = 0$ into (40) gives then immediately

$$K(x, 0) = K(x, L) = 0. \tag{41}$$

The case $\xi \approx x$ has again to be treated by means of a development in series which gives the result

$$K(x, \xi) \approx \frac{1}{2y} \left\{ \ln \frac{8y}{|x-\xi| \sqrt{(1-y'^2)}} + \frac{yy''}{1+y'^2} - 1 \right\} \text{ for } \xi \approx x. \tag{42}$$

$K(x, \xi)$ has a logarithmic singularity at $\xi = x$, i.e. is integrable. The finite part of $K(x, x)$ is discontinuous only, if $y''(x)$ is discontinuous, i.e. at the points where the curvature of the shape is discontinuous.

Now consider the cases $x = 0$ or $x = L$. The kernel has then to be determined as

$$K(0, \xi) = \lim_{x \to 0} K(x, \xi) \text{ and } K(L, \xi) = \lim_{x \to L} K(x, \xi). \tag{43}$$

According to (39a), the modulus k of the elliptic integrals in K will be small for small values of y. The integrals $K(k)$ and $E(k)$ can therefore be replaced approximately by

$$K(k) \approx \frac{\pi}{2} \left(1 + \frac{k^2}{4} + \frac{9}{64} k^4 \right); \; E(k) \approx \frac{\pi}{2} \left(1 - \frac{k^2}{4} - \frac{3}{64} k^4 \right). \tag{44}$$

The introduction of (44) into (39) gives the results

$$K(0, \xi) = \frac{\pi\eta^2}{(\xi^2+\eta^2)^{3/2}} \left\{ 1 - \frac{\frac{3}{4}\xi}{\xi^2 + \eta^2} \lim_{x \to 0} 2yy' \right\} \tag{45}$$

$$K(L, \xi) = \frac{\pi\eta^2}{\{(L-\xi)^2 + \eta^2\}^{3/2}} \left\{ 1 - \frac{\frac{3}{4}(L-\xi)}{(L-\xi)^2 + \eta^2} \lim_{x \to L} 2yy' \right\}. \tag{46}$$

4.3. *Solution of Linear Integral Equations*

The usual method for the solution of linear integral equations of the form (17)

$$\gamma^*(x) = 2 - \frac{1}{\pi}\int_0^L \gamma^*(\xi)K(x, \xi)d\xi \tag{47}$$

is an expansion of $\gamma^*(x)$ in powers of the 'parameter' $\lambda = -1/\pi$. This expansion is obtained by repeated integrations.

$$\gamma^*(x) = 2 - \frac{2}{\pi}\int_0^L K(x, \xi_1)d\xi_1 + \frac{2}{\pi^2}\int_0^L\int_0^L K(\xi_1, \xi_2)d\xi_2 K(x, \xi_1)d\xi_1 - \ldots . \tag{48}$$

The series (48) is convergent, if

$$\frac{1}{\pi} < |\lambda_0| , \tag{49}$$

where λ_0 denotes the smallest eigen value of $K(x, \xi)$. The rapidity of the convergence depends of course on the ratio $1/\pi : |\lambda_0|$.

As an estimation of λ_0 is rather difficult, some special cases will be considered, where the solution of equation (17) is known. The behaviour of the series (48) in these cases will give sufficient information for all cases of practical interest.

Consider first the two-dimensional flow past a *circular cylinder*. The introduction of

$$y = \sqrt{(1-x^2)},\ 2yy' = -2x \tag{50}$$

into the kernel of (17) (equation 24) gives the result

$$K(x, \xi) = \frac{2\sqrt{(1-\xi^2)}\,\{(x-\xi)^2 + x^2 - \xi^2 - 2x(x-\xi)\}}{[(x-\xi)^2 + \{\sqrt{(1-x^2)} + \sqrt{(1-\xi^2)}\}^2]\,[(x-\xi)^2 + \{\sqrt{(1-x^2)} - \sqrt{(1-\xi^2)}\}^2]} \equiv 0 . \tag{51}$$

$K(x, \xi)$ being identically zero in this particular case, the iterated kernels of the series (48) are equally zero, and the solution of (17) is

$$\gamma^*(x) = 2 + 0 + 0 + \ldots = 2 \tag{52}$$

$$w^*(x) = \frac{\gamma^*(x)}{\sqrt{(1+y'^2)}} = 2\sqrt{(1-x^2)} = 2\sin\phi \tag{53}$$

with

$$x = \cos\phi . \tag{54}$$

This is in fact the well-known velocity distribution of a circular cylinder.

The series (48) may therefore be expected to converge rather quickly for a shape $y(x)$ which does not differ too much from a circle, i.e. for fairly thick profiles.

In the corresponding three-dimensional case of the flow past a sphere, the velocity distribution is known to be

$$w^*(x) = \frac{3}{2}\sqrt{(1-x^2)} . \tag{55}$$

The solution of the integral equation (17) is therefore in this case

$$\gamma^*(x) = \frac{3}{2} . \tag{56}$$

Introducing this solution into (17), the value of the integral $\int K d\xi$ is obtained

$$\frac{3}{2} = 2 - \frac{1}{\pi}\int_{-1}^{+1} \frac{3}{2} K(x, \xi) d\xi \tag{57}$$

$$\frac{1}{\pi}\int_{-1}^{+1} K(x, \xi) d\xi = \frac{1}{3}. \tag{58}$$

The series (48) for γ^* will then be

$$\gamma^*(x) = 2 - \frac{2}{3} + \frac{2}{9} - \frac{2}{27} + \frac{2}{81} - + \ldots . \tag{59}$$

This series converging fairly quickly, a similar behaviour may be expected for rather short and thick bodies of revolution.

As there is more practical interest in elongated forms of profiles as well as of bodies of revolution, the flow along an *infinite circular cylinder* of diameter 2 or an *infinite plate* of thickness 2 will now be considered as an extreme case of this kind. Let therefore

$$y(x) \equiv 1 \text{ for } -\infty < x < \infty \tag{60}$$

in both the two-dimensional and the three-dimensional case. The boundary $y = 1$ being a streamline of the original parallel flow, the velocity $w(x)$ is obviously

$$w^*(x) \equiv 1 \tag{61}$$

and the solution of the integral equation is equally

$$\gamma^*(x) \equiv 1 \tag{62}$$

The integral equation (17) is reduced to

$$\gamma^*(x) = 2 - \frac{1}{\pi}\int_{-\infty}^{+\infty} \gamma^*(\xi) u^*(x, \xi) d\xi \tag{63}$$

in this case. Equations (62) and (63) give immediately the value of the integral

$$\frac{1}{\pi}\int_{-\infty}^{+\infty} u^*(x, \xi) d\xi \equiv 1 \tag{64}$$

in both the two-dimensional and the three-dimensional case.

With respect to (64), the series (48) for γ^* will then be

$$\gamma^*(x) = 2 - 2 + 2 - 2 + 2 - + \ldots \tag{65}$$

This series being of the oscillating type, a rather slow convergence of the series (48) may be expected in the practically most important cases of elongated profiles and bodies of revolution.

The convergence of the series (48) can, however, be greatly improved in these cases by a suitable transformation. Equation (48) can also be written in the form

$$\left.\begin{aligned} \gamma^*_0(x) &= 2 - \frac{1}{\pi}\int_0^L 2K(x, \xi) d\xi \\ \gamma^*_n(x) &= 2 - \frac{1}{\pi}\int_0^L \gamma^*_{n-1}(\xi) K(x, \xi) d\xi \\ \gamma^*(x) &= \lim_{n\to\infty} \gamma^*_n(x). \end{aligned}\right\} \tag{66}$$

Here, $\gamma^*(x)$ is obtained as the limit of the infinite sequence of functions $[\gamma^*_n(x)]$. If this sequence is convergent, the sequence

$$\left.\begin{aligned}
&\gamma^*_{01}(x) = 0;\ \gamma^*_{02}(x) = 2 - \frac{1}{\pi}\int_0^L \gamma^*_{01}(\xi)K(x,\xi)d\xi = 2\\
&\gamma^*_0(x) = \tfrac{1}{2}(\gamma^*_{01}+\gamma^*_{02}) = 1\\
&\gamma^*_{11}(x) = 2 - \frac{1}{\pi}\int_0^L \gamma^*_0(\xi)K(x,\xi)d\xi;\ \gamma^*_{12}(x) = \frac{1}{\pi}\int_0^L \gamma^*_{11}(\xi)K(x,\xi)d\xi\\
&\gamma^*_1(x) = \tfrac{1}{2}(\gamma^*_{11}+\gamma^*_{12})\\
&\gamma^*_{n1}(x) = 2 - \frac{1}{\pi}\int_0^L \gamma^*_{n-1}(\xi)K(x,\xi)d\xi;\ \gamma^*_{n2}(x) = 2 - \frac{1}{\pi}\int_0^L \gamma^*_n(\xi)K(x,\xi)d\xi\\
&\gamma^*_n(x) = \tfrac{1}{2}(\gamma^*_{n1}+\gamma^*_{n2})
\end{aligned}\right\} \qquad (67)$$

will have the same limit $\gamma^*(x)$, but its convergence will be more rapid in the case of an oscillating sequence (66).

An application of the scheme (67) to the case $y(x) \equiv 1$ gives immediately the solution

$$[\gamma^*_n(x)] = [1] \to \gamma^*(x) = 1. \qquad (68)$$

In practice, it may prove useful to use the schemes (66) and (67) together in different parts of the body. It will likewise be convenient to calculate in every step of these schemes only the difference between the improved function $\gamma^*_n(x)$ and the preceding approximation $\gamma^*_{n-1}(x)$. The iteration schemes (66) and (67) start from an estimated solution $\gamma \approx 2$ or 1, respectively. It will often be possible to use a better estimation in a particular case. This will reduce the number of steps necessary for obtaining the required degree of accuracy of the result.

5. *Formulae for the Velocity Outside the Body.*

The generation of a body by a vortex layer on its surface leads immediately to formulae expressing the velocity components at a point outside the body by the velocity distribution on its surface (Reference 7, Appendix).

Let (x, y) be a pivotal point in the field of flow outside the body and $w(\sigma)$ the velocity distribution on its surface Σ. The velocity components induced at (x, y) by the vortex layer on Σ will then be

$$u(x,y) = -\frac{1}{2\pi}\int_0^S w(\sigma)\,\frac{u^*\left\{\dfrac{x-\xi(\sigma)}{\eta(\sigma)}, \dfrac{y}{\eta(\sigma)}\right\}}{\eta(\sigma)}\,d\sigma \qquad (69)$$

$$v(x,y) = -\frac{1}{2\pi}\int_0^S w(\sigma)\,\frac{v^*\left\{\dfrac{x-\xi(\sigma)}{\eta(\sigma)}, \dfrac{y}{\eta(\sigma)}\right\}}{\eta(\sigma)}\,d\sigma. \qquad (70)$$

Here, u^* and v^* are again the non-dimensional velocity components of a vortex ring or pair, introduced in equations (9) and (19) (two-dimensional case) or (21) (three-dimensional case), respectively.

The pivotal point (x, y) being supposed to be outside the body, u^* and v^* are finite in the whole interval of integration. The numerical evaluation of these integrals presents therefore no difficulties.

6. *Numerical Examples.*

The general method developed in the preceding sections will now be used for the determination of the velocity distribution in the two-dimensional case of a semi-infinite plate with a semi-circular leading edge and in the three-dimensional case of a semi-infinite cylinder with three different heads (hemispherical, ogival and rounded). In all these cases, the curvature of the shape has discontinuities so that the method of singularities on the axis cannot be used.

The major part of the following numerical calculations is required for the computation of the kernel of the integral equation for a certain number of pivotal points on the surface. Special attention has therefore to be paid to a suitable selection of these points in order to obtain a sufficiently accurate result with only a small number of pivotal points. Generally, these points should be chosen fairly close to each other in all parts of the body, where irregularities of the velocity distribution can be expected (e.g. at a suction peak or at a discontinuity of the curvature); their spacing can be wider in the other parts of the body. The first step of the iteration procedure should be carried out with only a few pivotal points; their number is then increased in the following steps according to the requirements of the special problem. The variation of γ^* along the body is often smaller than the variation of w^*; the special form (17), (18) of the integral equation will then be more suitable for the numerical work than the general form (14).

6.1. *Two-Dimensional Case.*

Consider first the two-dimensional case of a semi-infinite plate of thickness 2, extending from $x = 1$ to $x = \infty$, with a front part in the form of a semi-circle (Fig. 4), i.e. let

$$y(x) = \begin{cases} \sqrt{2x - x^2} & \text{for } 0 < x < 1 \\ 1 & \text{for } 1 < x < \infty \,. \end{cases} \tag{71}$$

The kernel of the integral equation (17) for γ^* is obtained by introduction of equation (71) into the general form (24) of $K(x, \xi)$ in the two-dimensional case. This gives the formulae for $K(x, \xi)$ shown in Table 1 (opposite).

For the numerical calculation of the successive approximations $\gamma^*_n(x)$, the kernel $K(x, \xi)$ has first to be calculated for a certain number of pivotal points x. Fig. 5 gives some typical curves for $K(x, \xi)$.

In this figure, the relatively great difference between the curves $x = 0{\cdot}8$, $1{\cdot}0$ and $1{\cdot}2$ is to be noted from which a rather rapid variation of γ^* (and therefore of w^* too) near the point $x = 1$ may be expected. At this point, the radius of curvature of $y(x)$ is discontinuous ($\rho = 1$ for $x = 1 - 0$, $\rho = \infty$ for $x = 1 + 0$). It is in fact known that $w(x)$ has a vertical tangent at the points of discontinuity of ρ (Refs. 8 and 9). The general form of w at these points is

$$w \approx a + b(x - x_0) \ln |x - x_0| \,. \tag{72}$$

The most interesting part of the pressure distribution is its behaviour in the front part of the body between $x = 0$ and $x \sim 3$. In this part, the body may be considered as 'thick' so the scheme (66) was used for the calculation.

TABLE 1

Kernel of the Integral Equation for the Body of Figure 4
(Two-Dimensional Flow)

1. $x = 0$

$$K(0, \xi) = \begin{cases} 0 & \text{for } 0 < \xi < 1 \\ \dfrac{2(\xi-1)^2}{(\xi^2+1)^2} & \text{for } 1 < \xi < \infty . \end{cases} \tag{73}$$

2. $0 < x < 1$

$$K(x, \xi) = \begin{cases} 0 & \text{for } 0 < \xi < 1 \\ \dfrac{2(\xi-1)^2}{[(\xi-1)^2 + 2(1-x)(\xi-1) + 2]^2 - 4[1-(1-x)^2]} & \text{for } 1 < \xi < \infty . \end{cases} \tag{74}$$

3. $x = 1$

$$K(1, \xi) = \begin{cases} 0 & \text{for } 0 < \xi < 1 \\ 0 & \text{for } \xi = 1 - 0 \\ \frac{1}{2} & \text{for } \xi = 1 + 0 \\ \dfrac{2}{(1-\xi)^2 + 4} & \text{for } 1 < \xi < \infty . \end{cases} \tag{75}$$

4. $1 < x < \infty$

$$K(x, \xi) = \begin{cases} \dfrac{2(x-1)\,[(x-1) + 2(1-\xi)]\sqrt{\{1-(1-\xi)^2\}}}{[(x-\xi)^2 + 2 - (1-\xi)^2]^2 - 4[1-(1-\xi)^2]} & \text{for } 0 < \xi < 1 \\ \dfrac{2}{(x-1)^2 + 4} & \text{for } \xi = 1 \\ \dfrac{2}{(x-\xi)^2 + 4} & \text{for } 1 < \xi < \infty . \end{cases} \tag{76}$$

A suitable estimation for γ^*_0 is in this case

$$\gamma^*_0(x) = \begin{cases} 2 & \text{for } 0 < x < 1 \\ 1 & \text{for } 1 < x < \infty , \end{cases} \tag{77}$$

i.e. the exact solution for a circular cylinder on the semi-circular part and the exact solution for an infinite plate on the straight part.

With the aid of this estimated approximation, two further approximations

$$\gamma^*_1(x) = 2 - \frac{1}{\pi}\int_0^\infty \gamma^*_0(\xi) K(x, \xi)\, d\xi \tag{78}$$

$$\gamma^*_2(x) = 2 - \frac{1}{\pi}\int_0^\infty \gamma^*_1(\xi) K(x, \xi)\, d\xi \tag{79}$$

were calculated. The evaluation of the integrals was carried out numerically for the range $0 < \xi < 10$, the influence of the range from $\xi = 10$ to infinity was estimated by using the asymptotic behaviour of the kernel and of γ^*.

$$K(x, \xi) \to \frac{2}{(x-\xi)^2} \tag{80}$$

$$\gamma^*(x) \to 1 \tag{81}$$

The result of this calculation is shown in Fig. 6. The difference between γ^*_2 and γ^*_1 is small compared with the difference between γ^*_1 and γ^*_0; a further step in the iteration procedure will therefore give a result which is practically not different from γ^*_2.

It may be noted that the curve $\gamma^*_2(x)$ is outside the region between γ^*_0 and γ^*_1 in $0 \leqslant x < 1$ and between γ^*_0 and γ^*_1 for $x > 1$. This means that the successive approximations are likely to tend monotonically to γ^* in the front part of the body and to oscillate about γ^* in its rear part. This behaviour was in fact to be expected from the general discussion of the iteration procedure in Section 4.3.

The behaviour of $\gamma^*(x)$ near $x = 1$ is in good agreement with the behaviour which was to be expected from (72), though of course a decision whether the tangent of $\gamma^*(x)$ is really vertical at $x = 1$ or not, could not be obtained by the limited accuracy of the numerical integrations.

From $\gamma^*(x) \approx \gamma^*_2(x)$, the velocity $w^*(x)$ and the pressure p/q were calculated

$$\frac{w(x)}{V} = \frac{\gamma^*(x)}{\sqrt{(1+y'^2)}} = \begin{cases} \gamma^*(x)\sqrt{(2x-x^2)} & \text{for } 0 < x < 1 \\ \gamma^*(x) & \text{for } 1 < x < \infty \end{cases} \tag{82}$$

$$\frac{p}{q} = 1 - \left(\frac{w}{V}\right)^2. \tag{83}$$

The result is shown in Fig. 7. For comparison, the pressure distribution of a circular cylinder is also drawn in this figure (dotted line). The minimum of the pressure is of course smaller for the body than for the circular cylinder ($\sim -1{\cdot}65$ instead of -3), its position is slightly moved towards the bow ($x \sim 0{\cdot}8$ instead of $1{\cdot}0$). The discontinuity of the curvature causes, however, a rather rapid increase of the pressure near $x = 1$ which may affect the boundary layer.

6.2. *Three-Dimensional Case.*

In the three-dimensional case, special attention has to be paid to a suitable arrangement of the numerical calculation in order to reduce the considerable numerical work as far as possible. For simplicity, the following general remarks will be restricted to the special form (17) of the integral equation and to the iteration scheme (66); the more general form (14) of the integral equation and the iteration scheme (67) do not present any new difficulties.

At first the kernel has to be calculated for a certain number of pivotal points x, selected according to the general remarks in Section 6.1. The form

$$K(x, \xi) = \frac{u^*\left(\frac{x-\xi}{\eta}, \frac{y}{\eta}\right) + y' v^*\left(\frac{x-\xi}{\eta}, \frac{y}{\eta}\right)}{\eta} \tag{84}$$

of the kernel (17), together with its development (42) for $\xi \approx x$, could be considered as suitable for the calculation, as tables for u^* and v^* have been computed (Ref. 6). These tables being, however, largely obtained by graphical interpolation from a relatively small number of calculated

points, their accuracy is not always sufficient for the present purpose. Moreover, their intervals were found to be still too wide for the necessary double interpolation at a distance from $\xi = x$, where the development (42) could no longer be used.

Generally, the use of Küchemann's tables becomes difficult, if the distance between the variable point (ξ, η) and the pivotal point (x, y) is smaller than about $0{\cdot}5\,\eta$. For the present purpose, the tables were only used for values of ξ on the cylindrical part of the body. Here, the kernel can be calculated once for all, if the pivotal points on the curved head are selected so that y has certain fixed values.

Table 2 gives the values of u^*/π and v^*/π on the cylindrical part of the body as functions of $(x-\xi)/\eta_{\mathrm{cyl}}$ for different values of y/η_{cyl}. The scale of $(x-\xi)/\eta_{\mathrm{cyl}}$ is at first quadratic {for $0 > (x-\xi)/\eta_{\mathrm{cyl}} > 1$} in order to facilitate the numerical treatment of the singularity of the kernel $K(x, \xi)$ which is discussed below. In this part of the table, interpolation is not advisable, at least not in the direction of $x - \xi$. If more points are required, they can be calculated with the aid of (21) and (21a). The values of u^*/π and v^*/π are given until $(x-\xi)/\eta_{\mathrm{cyl}} = -10$. For $(x-\xi)/\eta_{\mathrm{cyl}} < -10$, u^* and v^* are approximately

$$\frac{u^*}{\pi} \approx \left|\frac{x-\xi}{\eta_{\mathrm{cyl}}}\right|^{-3} \tag{85}$$

$$\frac{v^*}{\pi} \approx -\frac{3}{2}\frac{y}{\eta_{\mathrm{cyl}}}\left(\frac{x-\xi}{\eta_{\mathrm{cyl}}}\right)^{-4}. \tag{86}$$

The last line of Table 2 gives the values of the integrals of u^*/π and v^*/π from -10 to $-\infty$, calculated from (85) and (86).

For the calculation of $K(x, \xi)$ on the curved part of the surface, (40) and (42) are suitable. Near $\xi = x$, but outside the range of validity of (42), it is convenient to use the complementary modulus

$$k'^2 = 1 - k^2 = \frac{(x-\xi)^2 + (y-\eta)^2}{(x-\xi)^2 + (y+\eta)^2} \tag{87}$$

instead of k^2 (39a) for the determination of the elliptic integrals K and E in (40). The Tables 3, 4 and 4a give the values of E/π and $(K-E)/\pi$ functions of k^2 and k'^2. For more-accurate tables see Refs. 10 and 11. A calculation with three figures will often be sufficient, more than four figures will be necessary only in exceptional cases.

A certain difficulty in the use of equation (40) near $\xi = x$ is the calculation of the factor of $E(k^2)$

$$F = \frac{2\eta[y - \eta - y'(x-\xi)]}{(x-\xi)^2 + (y-\eta)^2}. \tag{88}$$

For $x = \xi$, F has the form 0/0 with the finite limit

$$\lim_{\xi \to x} F = -\frac{yy''}{1+y'^2}, \tag{89}$$

i.e. its calculation requires a rather good knowledge of y' and y''. If the shape is given by a simple analytical equation, the calculation of y' and y'' is in general not difficult. Sometimes, it will then even be possible to transform F analytically so that it has no longer the form 0/0 for $\xi = x$. This is the case if, for example, the shape is given in the form of a polynomial in x or $x^{1/2}$, or if it is composed of arcs of circles as in the three following examples (Fig. 8). In this latter case, F is simply

$$F = \frac{\eta}{y-b} \quad \text{for} \quad \begin{aligned} y &= b + \sqrt{\{r^2 - (x-a)^2\}} \\ \eta &= b + \sqrt{\{r^2 - (\xi-a)^2\}}. \end{aligned} \tag{90}$$

If a simple analytical equation for the shape does not exist, it will always be possible to find a sufficiently accurate interpolation formula for a certain neighbourhood of $x = \xi$ and to use this formula for the determination of F.

Another difficulty is the numerical evaluation of the integrals of ${\gamma^*}_n K(x, \xi)$ in the neighbourhood of the singularity $\xi = x$. This singularity can be removed by a suitable transformation of ξ (*see* Ref. 12, Appendix). Let

$$\int_0^\infty {\gamma^*}_n(\xi) K(x, \xi) d\xi = \int_0^a + \int_a^x + \int_x^b + \int_b^\infty \tag{91}$$

where a and b are arbitrary values between 0 and x or x and ∞. The integrands of the second and third integral are infinite at $\xi = x$. With the substitutions

$$x - \xi = \chi^2 \qquad d\xi = -2\chi d\chi, \tag{92}$$

or

$$\xi - x = \chi^2 \qquad d\xi = 2\chi d\chi, \tag{93}$$

respectively, these integrals become

$$\int_0^{\sqrt{(x-a)}} {\gamma^*}_n K 2\chi d\chi \text{ and } \int_0^{\sqrt{(b-x)}} {\gamma^*}_n K 2\chi d\chi. \tag{94}$$

The behaviour of the transformed integrands near $\chi = 0$ will now be

$${\gamma^*}_n K 2\chi \sim \text{const. } \chi \log \chi \to 0 \text{ as } \chi \to 0. \tag{95}$$

The integrals can therefore be determined by the usual numerical methods. A suitable choice of the interval $|x - a|$ to $|x - b|$ is a length equal to the radius of the cylinder.

The infinite interval of integration in the last term of (91) can be transformed into a finite interval in a similar manner (substitution $\xi = \chi^{-1}$). It is, however, sufficient in this case to calculate the integral for a suitable finite interval (about 5 diameters of the body) and to estimate the small contribution of the remaining part from (85), (86) and the asymptotic behaviour $\gamma^* \to 1$ of the solution.

(a) *Hemispherical Head.*

In the case of a hemispherical head (Fig. 8a), the shape of the body is given by

$$y(x) = \begin{cases} \sqrt{(2x - x^2)} & \text{for } 0 < x < 1 \\ 1 & \text{for } 1 < x < \infty. \end{cases} \tag{96}$$

y being a univalued function of x and the form (17) of the integral equation can be used. The iteration scheme (66) is likely to be suitable for the numerical solution of (17), as the body can be considered as 'thick' in its front part, where the pressure distribution is required.

Some typical curves for the kernel of the integral equation are drawn in Fig. 9. As in the corresponding two-dimensional case (Fig. 5), the curves $x = 0{\cdot}8$, 1 and $1{\cdot}2$ show a considerable difference in their area, though not so obviously, due to the influence of the singularity. A rather rapid decrease of γ^* may therefore again be expected near $x = 1$.

The transformation (92), (93), of the kernel for the numerical treatment of its singularity is shown in Fig. 10. For the numerical determination of the integrals of $\gamma^*_n K$, the transformed kernel has to be multiplied by γ^*_n; the integrals can then by evaluated either graphically or numerically.

For the determination of the successive approximations γ^*_n of the solution γ^* of (17), γ^*_0 was estimated to be

$$\gamma^*_0(x) = \begin{cases} 1{\cdot}5 & \text{for } 0 < x < 1 \\ 1 & \text{for } 1 < x < \infty\,, \end{cases} \tag{97}$$

i.e. the exact solution for a sphere on the spherical part and the exact solution for an infinite cylinder on the cylindrical part of the body. With this estimated solution, two further approximations γ^*_1 and γ^*_2 were calculated from (66)

$$\gamma^*_1(x) = 2 - \int_0^\infty \gamma^*_0(\xi) K(x, \xi)\, d\xi \tag{98}$$

$$\gamma^*_2(x) = 2 - \int_0^\infty \gamma^*_1(\xi) K(x, \xi)\, d\xi\,. \tag{99}$$

The result is plotted in Fig. 11. The difference between γ^*_1 and γ^*_2 being small in comparison with the difference of γ^*_0 and γ^*_1, γ^*_2 could be considered as a sufficiently accurate approximation for γ^*.

With $\gamma^* \approx \gamma^*_2$, the velocity

$$w^*(x) = \frac{\gamma^*(x)}{\sqrt{(1+y'^2)}} = \begin{cases} \sqrt{(2x - x^2)}\gamma^*(x) & \text{for } 0 < x < 1 \\ \gamma^*(x) & \text{for } 1 < x < \infty \end{cases} \tag{100}$$

was calculated from equation (8). The pressure distribution of the body was then obtained from Bernoulli's equation

$$\frac{p - p_0}{\frac{\rho}{2} V^2} = 1 - w^*(x)^2\,. \tag{101}$$

The calculated pressure distribution is plotted in Fig. 12, together with experimental results of H. Rouse, J. S. McNown and En-Yun Hsu (Ref. 13a), obtained in an open-jet water tunnel of 13 in. diameter with a model of 1 in. diameter (Reynolds number $Vd/\nu = 2 \times 10^5$).

The agreement of theory and experiment is almost complete in this figure. The only experimental point which does not quite fall on the theoretical curve, is at $x = 1$, where the hemisphere is attached to the cylinder. This behaviour which is also to be observed in the following examples, was to be expected from theoretical considerations (cf. Ref. 9), as the boundary layer will somewhat smooth the rapid increase of the pressure at the points of discontinuous curvature where the theoretical pressure distribution has a vertical tangent. The small size of the model used in the experiments makes it, however, difficult to separate the influence of the boundary layer from that of experimental errors and inevitable imperfections of the model as the horizontal distance of the experimental point from the theoretical curve is only about 1/25 in. in actual size, and the diameter of the pressure hole was of the same order of magnitude (1/32 in.).

(b) 2 *Caliber Ogival Head.*

In the case of a 2 caliber ogival head (Fig. 8b), the shape of the body is given by

$$y = \begin{cases} +\sqrt{\{16-(\sqrt{7}-x)^2\}}-3 & \text{for} \quad 0<x<\sqrt{7} \\ 1 & \text{for} \quad \sqrt{7}<x<\infty\,. \end{cases} \tag{102}$$

As in the preceding example, y is again a univalued function of x. The form (17) of the integral equation can therefore be used for the numerical work. But contrary to the case of a hemispherical head, the front part of the body has now to be considered as elongated; the iteration scheme (67) will therefore be more suitable than (66) for the solution.

A suitable estimation for γ^*_0 is simply

$$\gamma^*_0(x) \equiv 1 \tag{103}$$

which is likely to give rather small corrections almost everywhere on the body, except in the immediate neighbourhood of its bow $x = 0$, where the solution $\gamma^*(x)$ must be zero. With $\gamma^*_0 \equiv 1$, the first approximation

$$\left.\begin{aligned} \gamma^*_{11}(x) &= 2-\int_0^\infty K(x,\xi)d\xi \\ \gamma^*_{12}(x) &= 2-\int_0^\infty \gamma_{11}(\xi)K(x,\xi)d\xi \\ \gamma^*_1(x) &= \tfrac{1}{2}(\gamma^*_{11}+\gamma^*_{12}) \end{aligned}\right\} \tag{104}$$

was calculated (Fig. 13). Several points of the following approximation γ^*_{21} were then calculated and found to be practically on the curve $\gamma^*_1(x)$ (small circles in Fig. 13). $\gamma^*_1(x)$ could therefore be considered as a sufficiently accurate solution of the integral equation.

With $\gamma^*(x) \approx \gamma^*_1(x)$, the pressure distribution of the body was calculated from

$$w^*(x) = \frac{\gamma^*(x)}{\sqrt{(1+y'^2)}} = \begin{cases} \gamma^*(x)\sqrt{\left\{1-\left(\dfrac{\sqrt{7}-x}{4}\right)^2\right\}} & \text{for } 0 \leqslant x \leqslant \sqrt{7} \\ \gamma^*(x) & \text{for } \sqrt{7} < x < \infty \end{cases} \tag{105}$$

and Bernoulli's equation (101). The result is plotted in Fig. 14 and compared with the experimental results of Rouse, McNown and Hsu (Reynolds number 2×10^5, Ref. 13b). As in the preceding example, the agreement of theory and experiment is almost complete, with the exception of the transition from the curved head to the cylinder ($x = \sqrt{7}$). The rapid increase of the theoretical pressure curve is here again somewhat smoothed by the influence of the boundary layer.

(c) *Flat Head.*

In the case of a flat head with a $\frac{1}{4}$ caliber radius (Fig. 8c), the shape of the body cannot be described by an equation $y = y(x)$, as $y(x)$ would not be a univalued function at the bow $x = 0$. The calculation has therefore to be based on the general form (14) of the integral equation for $w^*(s)$. The iteration scheme (66) is likely to be suitable for the numerical work, as the body can be considered as 'thick' in its front part.

Introducing the length of arc s of the shape, the co-ordinates of a point (x, y) on the surface and their derivatives with respect to s become

$$\left.\begin{aligned} y(s) &= s\,,\ x(s) = 0 \\ \frac{dy}{ds} &= 1\,,\ \frac{dx}{ds} = 0 \end{aligned}\right\} \text{ for } 0 < s < \tfrac{1}{2} \tag{106a}$$

$$\left.\begin{aligned} y(s) &= \tfrac{1}{2}[1 + \sin(2s-1)]\,,\ x(s) = \tfrac{1}{2}[1 - \cos(2s-1)] \\ \frac{dy}{ds} &= \cos(2s-1)\,,\ \frac{dx}{ds} = \sin(2s-1) \end{aligned}\right\} \text{ for } \tfrac{1}{2} < s < \tfrac{1}{2} + \frac{\pi}{4} \tag{106b}$$

$$\left.\begin{aligned} y(s) &= 1\,,\ x(s) = S - \frac{\pi}{4} \\ \frac{dy}{ds} &= 0\,,\ \frac{dx}{ds} = 1 \end{aligned}\right\} \text{ for } \tfrac{1}{2} + \frac{\pi}{4} < s < \infty\,. \tag{106c}$$

The calculation of the kernel of (14) can be carried out as in the preceding examples and does not present any difficulties.

A good estimation w^*_0 of the solution of (14) seems rather difficult. Fortunately the iteration converges so quickly that even a considerable difference between w^*_0 and w^* in the front part is not very important. w^* will increase from zero at the stagnation point $s = 0$ to a maximum value greater than 1 somewhere on the curved part, then decrease again and tend rather quickly towards its asympotic value 1 on the cylindrical part. w^*_0 was therefore estimated as

$$w^*_0(s) = \begin{cases} 3s \text{ on the flat front disc } (0 < s < \tfrac{1}{2}) \\ 1{\cdot}5 \text{ on the rounded part } \left(\tfrac{1}{2} < s < \tfrac{1}{2} + \frac{\pi}{4}\right) \\ 1 \text{ on the cylindrical part } \left(\tfrac{1}{2} + \frac{\pi}{4} < s < \infty\right). \end{cases} \tag{107}$$

With this estimated solution, two further approximations w^*_1 and w^*_2 were calculated, using the iteration scheme (66). The result is shown in Fig. 15. On the front part of the body, the difference between w^*_0 and w^*_1 is still rather great. Nevertheless, the difference between w^*_2 and w^*_1 is very small, and so small in comparison with $w^*_0 - w^*_1$ that w^*_2 can be considered as a sufficiently accurate solution of the integral equation (14).

The pressure distribution was then calculated from Bernoulli's equation with $w^* \approx w^*_2$ (Fig. 16). The comparison of the theoretical curve and the experimental results of Rouse, McNown and Hsu (Reynolds number 2×10^5, Ref. 13c) shows again a very good agreement between theory and experiment.

7. *Conclusion.*

The direct iteration method described in the present report has proved suitable for the determination of the pressure distribution of symmetrical profiles and of bodies of revolution in longitudinal flow. The amount of numerical work required for this method being, however, rather

great, it will be restricted, from the practical point of view, to cases where the indirect methods are bound or at least likely to fail. This is especially the case, if the bow of the body is too blunt or if its shape is composed of arcs of different curves, e.g. circles and straight lines.

The method was used for the calculation of the pressure distribution of a semi-infinite plate with a semi-circular leading edge and of a semi-infinite cylinder with heads of various shapes (hemispherical, 2 caliber ogival, $\frac{1}{4}$ caliber rounded). In the latter case, the theoretical results could be compared with experiments. The agreement was found to be very close. Near the transition from the head to the cylinder, where the curvature of the shape is discontinuous, the theory gives a rather rapid increase of the pressure curve with a vertical tangent at the transition point. The experiments show that this rapid increase is somewhat smoothed in an actual fluid due to the influence of the boundary layer.

It is of some interest to compare the minimum pressure of a cylinder $(p-p_0)_{\min} = \{-3(\frac{1}{2}\rho V^2)\}$ with that of the semi-infinite plate with a semi-circular leading edge $\{-1{\cdot}65(\frac{1}{2}\rho V^2)\}$ and the minimum pressure of a sphere $\{-1{\cdot}25(\frac{1}{2}\rho V^2)\}$ with that of the semi-infinite cylinder with a hemispherical head $\{-0{\cdot}77(\frac{1}{2}\rho V^2)\}$. In each case, the minimum pressure is considerably reduced by the influence of the attached straight part (-48% and -38%). A similar behaviour may be expected for other shapes of the head, if the body obtained by symmetrical continuation of the head with respect to the point where it is attached to the cylinder, has its minimum pressure at the centre. A suction peak near the bow of the head is of course likely to be less affected by the influence of the straight cylindrical part.

REFERENCES

No.	Author(s)	Title, etc.
1	Th. von Kármán	Berechnung der Druckverteilung von Luftschiffkorpern. Abh. aero. Inst. tech. Hochsch., Aachen, Part 7, pp. 3 to 17. Jul. Springer, Berlin. 1927.
2	C. Kaplan	Potential flow about elongated bodies of revolution. N.A.C.A. Report 516. 1935.
3	L. Prandtl and O. Tietjens ..	*Hydro-und Aeromechanik.* Vol. 1. Jul. Springer, Berlin. 1929.
4	L. Prandtl	Tragflugeltheorie. Part I of *Vier Abhandlungen zur Hydrodynamik und Aerodynamik*, L. Prandtl and A. Betz, Göttingen. 1927.
5	H. Lamb	*Hydrodynamics.* 6th Edition, Cambridge University Press. 1932.
6	D. Küchemann	Tafeln für die Stromfunktion und die Geschwindikeitskomponenten von Quellring und Wirbelring. *Jb. dtsch. Luftfahrtforsch.*, Vol. 1, p. 547. 1940.
7	J. H. Preston	The effect of the boundary layer and wake on the flow past a symmetrical aerofoil at zero incidence. Part I. A.R.C. R. & M. 2107. July, 1945.
8	W. V. Koppenfels	Ebene Potentialstromung langs einer glatten Wand mit stuckweise stetiger Krummung. *Luftfahrtforsch.*, Vol. 19, p. 129. 1942.
9	A. Betz	Verlauf der Stromungsgeschwindigkeit in der Naehe einer Wand bei unstetiger Anderung der Krummung. *Luftfahrtforsch.*, Vol. 19, p. 129. 1942.
10	E. Jahnke and F. Emde ..	*Tafeln höherer Funktionen.* Vierte Auflage, Leipzig. 1948.
11	H. B. Dwight	Mathematical tables. McGraw-Hill Book Co. Inc., New York and London. 1944.
12	F. Vandrey	Zur theoretischen Behandlung des gegenseitigen Einflusses von Tragflügel und Rumpf. *Luftfahrtforsch.*, Vol. 14, p. 347. 1937.
13	H. Rouse, J. S. McNown and En-Yun Hsu.	Cavitation tests on a symmetric series of torpedo heads. (*a*) Hemispherical head. (*b*) 2 caliber ogival head. (*c*) $\frac{1}{4}$ caliber rounded head. Iowa Institute of Hydraulic Research, State University of Iowa, Iowa City. March, 1945.

TABLE 2

u^*/π and v^*/π on the Cylindrical Part of the Body for the Calculation of $K = (u^* + y'v^*)/\pi\eta$

$\frac{x-\xi}{\eta_{cyl}}$	$\frac{y}{\eta_{cyl}} = 1$	$\frac{y}{\eta_{cyl}} = 0{\cdot}99$		$\frac{y}{\eta_{cyl}} = 0{\cdot}95$	
	$\frac{1}{\pi}u^*$	$\frac{1}{\pi}u^*$	$\frac{1}{\pi}v^*$	$\frac{1}{\pi}u^*$	$\frac{1}{\pi}v^*$
0	∞	32·9	0	7·20	0
− 0·01	0·905	16·9	−25·12	6·94	−1·25
− 0·04	0·684	2·57	−11·79	4·61	−3·17
− 0·09	0·554	0·947	− 5·46	2·09	−2·73
− 0·16	0·462	0·588	− 3·04	1·048	−1·80
− 0·25	0·389	0·442	− 1·89	0·646	−1·17
− 0·36	0·328	0·354	− 1·25	0·457	−0·788
− 0·49	0·276	0·290	− 0·859	0·347	−0·541
− 0·64	0·230	0·238	− 0·599	0·272	−0·376
− 0·81	0·189	0·194	− 0·420	0·215	−0·262
− 1·00	0·154	0·157	− 0·294	0·170	−0·182
− 1·2	0·124	0·126	− 0·208	0·135	−0·128
− 1·4	0·101	0·103	− 0·151	0·109	−0·0920
− 1·6	0·0830	0·0840	− 0·111	0·0880	−0·0674
− 1·8	0·0683	0·0691	− 0·0832	0·0720	−0·0501
− 2·0	0·0567	0·0572	− 0·0632	0·0593	−0·0380
− 2·2	0·0448	0·0477	− 0·0485	0·0492	−0·0290
− 2·4	0·0397	0·0400	− 0·0386	0·0411	−0·0225
− 2·6	0·0336	0·0338	− 0·0298	0·0346	−0·0177
− 2·8	0·0285	0·0287	− 0·0236	0·0294	−0·0131
− 3·0	0·0244	0·0246	− 0·0190	0·0250	−0·0113
− 3·2	0·0210	0·0212	− 0·0153	0·0215	−0·0091
− 3·4	0·0182	0·0183	− 0·0126	0·0186	−0·0074
− 3·6	0·0158	0·0159	− 0·0104	0·0161	−0·0061
− 3·8	0·0138	0·0139	− 0·0086	0·0141	−0·0050
− 4·0	0·0122	0·0122	− 0·0072	0·0124	−0·0042
− 4·5	0·0090	0·0090	− 0·0048	0·0091	−0·0029
− 5·0	0·0068	0·0068	− 0·0033	0·0068	−0·0019
− 5·5	0·0052	0·0052	− 0·0024	0·0052	−0·0013
− 6·0	0·0041	0·0041	− 0·0017	0·0041	−0·0010
− 6·5	0·0033	0·0033	− 0·0013	0·0033	−0·0007
− 7·0	0·0027	0·0027	− 0·0010	0·0027	−0·0006
− 7·5	0·0022	0·0022	− 0·0007	0·0022	−0·0005
− 8·0	0·0018	0·0018	− 0·0005	0·0018	−0·0004
− 8·5	0·0015	0·0015	− 0·0004	0·0015	−0·0003
− 9·0	0·0013	0·0013	− 0·0003	0·0013	−0·0002
− 9·5	0·0011	0·0011	− 0·0003	0·0011	−0·0002
−10·0	0·0010	0·0010	− 0·0002	0·0010	−0·0001
$\frac{1}{\pi}\int_{x/\eta_{cyl}+10}^{\infty} v^* d\frac{\xi}{\eta_{cyl}}$	0·0050	0·0050	− 0·0005	0·0050	−0·0005

TABLE 2—*continued*

$\frac{x-\xi}{\eta_{cyl}}$	$\frac{y}{\eta_{cyl}} = 0{\cdot}90$		$\frac{y}{\eta_{cyl}} = 0{\cdot}85$		$\frac{y}{\eta_{cyl}} = 0{\cdot}80$	
	$\frac{1}{\pi}u^*$	$\frac{1}{\pi}v^*$	$\frac{1}{\pi}u^*$	$\frac{1}{\pi}v^*$	$\frac{1}{\pi}u^*$	$\frac{1}{\pi}v^*$
0	3·93	0	2·82	0	2·26	0
− 0·01	3·89	−0·327	2·79	−0·148	2·25	−0·0842
− 0·04	3·45	−1·138	2·66	−0·555	2·19	−0·324
− 0·09	2·37	−1·629	2·18	−0·976	1·94	−0·626
− 0·16	1·40	−1·445	1·52	−1·084	1·51	−0·802
− 0·25	0·858	−1·070	1·001	−0·925	1·08	−0·775
− 0·36	0·577	−0·758	0·677	−0·704	0·754	−0·637
− 0·49	0·417	−0·532	0·481	−0·512	0·537	−0·483
− 0·64	0·314	−0·373	0·355	−0·365	0·393	−0·352
− 0·81	0·242	−0·261	0·267	−0·256	0·293	−0·250
− 1·00	0·187	−0·181	0·204	−0·178	0·220	−0·174
− 1·2	0·146	−0·127	0·159	−0·126	0·171	−0·125
− 1·4	0·116	−0·0908	0·124	−0·0889	0·133	−0·0869
− 1·6	0·0932	−0·0661	0·0986	−0·0647	0·104	−0·0634
− 1·8	0·0755	−0·0491	0·0790	−0·0480	0·0825	−0·0468
− 2·0	0·0618	−0·0370	0·0644	−0·0359	0·0669	−0·0347
− 2·2	0·0511	−0·0283	0·0530	−0·0272	0·0548	−0·0261
− 2·4	0·0425	−0·0219	0·0440	−0·0208	0·0454	−0·0197
− 2·6	0·0357	−0·0171	0·0367	−0·0163	0·0376	−0·0154
− 2·8	0·0301	−0·0134	0·0308	−0·0127	0·0315	−0·0120
− 3·0	0·0257	−0·0108	0·0263	−0·0102	0·0268	−0·0097
− 3·2	0·0220	−0·0088	0·0225	−0·0083	0·0230	−0·0078
− 3·4	0·0190	−0·0071	0·0193	−0·0067	0·0196	−0·0064
− 3·6	0·0164	−0·0058	0·0167	−0·0056	0·0169	−0·0054
− 3·8	0·0143	−0·0049	0·0145	−0·0047	0·0147	−0·0046
− 4·0	0·0125	−0·0039	0·0127	−0·0038	0·0129	−0·0038
− 4·5	0·0092	−0·0026	0·0093	−0·0025	0·0094	−0·0024
− 5·0	0·0069	−0·0017	0·0070	−0·0018	0·0071	−0·0018
− 5·5	0·0053	−0·0013	0·0053	−0·0013	0·0053	−0·0013
− 6·0	0·0042	−0·0009	0·0042	−0·0009	0·0042	−0·0009
− 6·5	0·0033	−0·0007	0·0033	−0·0007	0·0033	−0·0007
− 7·0	0·0027	−0·0005	0·0027	−0·0005	0·0027	−0·0005
− 7·5	0·0022	−0·0004	0·0022	−0·0004	0·0022	−0·0004
− 8·0	0·0018	−0·0003	0·0018	−0·0004	0·0018	−0·0004
− 8·5	0·0015	−0·0002	0·0015	−0·0003	0·0015	−0·0003
− 9·0	0·0013	−0·0002	0·0013	−0·0002	0·0013	−0·0002
− 9·5	0·0011	−0·0001	0·0011	−0·0002	0·0011	−0·0002
−10·0	0·0010	−0·0001	0·0010	−0·0001	0·0010	−0·0001
$\frac{1}{\pi}\int_{x/\eta_{cyl}+10}^{\infty} \begin{matrix} u^* \\ v^* \end{matrix} d\frac{\xi}{\eta_{cyl}}$	0·0050	−0·0005	0·0050	−0·0004	0·0050	−0·0004

TABLE 2—*continued*

$\frac{x-\xi}{\eta_{cyl}}$	$\frac{y}{\eta_{cyl}} = 0{\cdot}75$		$\frac{y}{\eta_{cyl}} = 0{\cdot}70$		$\frac{y}{\eta_{cyl}} = 0{\cdot}60$	
	$\frac{1}{\pi}u^*$	$\frac{1}{\pi}v^*$	$\frac{1}{\pi}u^*$	$\frac{1}{\pi}v^*$	$\frac{1}{\pi}u^*$	$\frac{1}{\pi}v^*$
0	1·92	0	1·69	0	1·41	0
− 0·01	1·92	−0·0542	1·69	−0·0377	1·41	−0·0209
− 0·04	1·88	−0·211	1·67	−0·148	1·40	−0·0828
− 0·09	1·74	−0·429	1·58	−0·308	1·36	−0·178
− 0·16	1·46	−0·601	1·38	−0·458	1·25	−0·282
− 0·25	1·11	−0·639	1·11	−0·524	1·08	−0·354
− 0·36	0·808	−0·565	0·843	−0·494	0·874	−0·369
− 0·49	0·584	−0·449	0·623	−0·411	0·675	−0·333
− 0·64	0·427	−0·335	0·458	−0·315	0·508	−0·269
− 0·81	0·316	−0·241	0·339	−0·230	0·377	−0·203
− 1·00	0·236	−0·169	0·251	−0·162	0·278	−0·146
− 1·2	0·182	−0·120	0·193	−0·114	0·213	−0·103
− 1·4	0·141	−0·0841	0·148	−0·0812	0·161	−0·0736
− 1·6	0·109	−0·0612	0·114	−0·0589	0·123	−0·0532
− 1·8	0·0858	−0·0449	0·0891	−0·0430	0·0955	−0·0385
− 2·0	0·0693	−0·0331	0·0716	−0·0315	0·0761	−0·0281
− 2·2	0·0565	−0·0249	0·0582	−0·0237	0·0615	−0·0209
− 2·4	0·0466	−0·0188	0·0477	−0·0178	0·0500	−0·0158
− 2·6	0·0385	−0·0146	0·0395	−0·0139	0·0411	−0·0123
− 2·8	0·0323	−0·0115	0·0331	−0·0109	0·0344	−0·0096
− 3·0	0·0274	−0·0092	0·0279	−0·0088	0·0288	−0·0078
− 3·2	0·0234	−0·0075	0·0237	−0·0071	0·0244	−0·0063
− 3·4	0·0200	−0·0061	0·0203	−0·0059	0·0208	−0·0053
− 3·6	0·0172	−0·0051	0·0174	−0·0049	0·0178	−0·0044
− 3·8	0·0149	−0·0043	0·0151	−0·0041	0·0154	−0·0036
− 4·0	0·0131	−0·0036	0·0132	−0·0034	0·0134	−0·0030
− 4·5	0·0094	−0·0023	0·0095	−0·0022	0·0097	−0·0019
− 5·0	0·0071	−0·0017	0·0071	−0·0016	0·0072	−0·0014
− 5·5	0·0054	−0·0012	0·0054	−0·0011	0·0055	−0·0010
− 6·0	0·0043	−0·0008	0·0043	−0·0008	0·0043	−0·0007
− 6·5	0·0034	−0·0006	0·0034	−0·0006	0·0034	−0·0005
− 7·0	0·0027	−0·0005	0·0027	−0·0005	0·0027	−0·0004
− 7·5	0·0022	−0·0004	0·0022	−0·0004	0·0022	−0·0003
− 8·0	0·0018	−0·0003	0·0018	−0·0003	0·0018	−0·0003
− 8·5	0·0015	−0·0003	0·0015	−0·0003	0·0015	−0·0002
− 9·0	0·0013	−0·0002	0·0013	−0·0002	0·0013	−0·0002
− 9·5	0·0011	−0·0002	0·0011	−0·0001	0·0011	−0·0001
−10·0	0·0010	−0·0001	0·0010	−0·0001	0·0010	−0·0001
$\frac{1}{\pi}\int_{x/\eta_{cyl}+10}^{\infty} \begin{matrix} u^* \\ v^* \end{matrix} d\frac{\xi}{\eta_{cyl}}$	0·0050	−0·0004	0·0050	−0·0004	0·0050	−0·0003

TABLE 2—*continued*

$\frac{x-\xi}{\eta_{cyl}}$	$\frac{y}{\eta_{cyl}} = 0{\cdot}50$		$\frac{y}{\eta_{cyl}} = 0{\cdot}40$		$\frac{y}{\eta_{cyl}} = 0{\cdot}30$	
	$\frac{1}{\pi} u^*$	$\frac{1}{\pi} v^*$	$\frac{1}{\pi} u^*$	$\frac{1}{\pi} v^*$	$\frac{1}{\pi} u^*$	$\frac{1}{\pi} v^*$
0	1·24	0	1·14	0	1·07	0
− 0·01	1·24	−0·0130	1·14	−0·0084	1·07	−0·0054
− 0·04	1·23	−0·0507	1·13	−0·0334	1·06	−0·0214
− 0·09	1·20	−0·111	1·10	−0·0719	1·04	−0·0468
− 0·16	1·14	−0·183	1·06	−0·121	1·02	−0·0780
− 0·25	1·03	−0·245	0·984	−0·166	0·952	−0·110
− 0·36	0·880	−0·272	0·866	−0·194	0·853	−0·135
− 0·49	0·708	−0·262	0·719	−0·196	0·727	−0·139
− 0·64	0·551	−0·220	0·573	−0·173	0·586	−0·127
− 0·81	0·411	−0·172	0·436	−0·139	0·452	−0·103
− 1·00	0·306	−0·127	0·324	−0·103	0·338	−0·0783
− 1·2	0·229	−0·0898	0·242	−0·0741	0·252	−0·0564
− 1·4	0·172	−0·0640	0·181	−0·0528	0·188	−0·0404
− 1·6	0·131	−0·0462	0·138	−0·0378	0·143	−0·0294
− 1·8	0·102	−0·0331	0·107	−0·0273	0·111	−0·0213
− 2·0	0·0802	−0·0243	0·0840	−0·0200	0·0866	−0·0157
− 2·2	0·0640	−0·0180	0·0666	−0·0148	0·0685	−0·0118
− 2·4	0·0519	−0·0135	0·0534	−0·0111	0·0551	−0·0087
− 2·6	0·0426	−0·0105	0·0439	−0·0087	0·0450	−0·0068
− 2·8	0·0353	−0·0083	0·0363	−0·0069	0·0369	−0·0054
− 3·0	0·0296	−0·0068	0·0304	−0·0056	0·0309	−0·0044
− 3·2	0·0251	−0·0056	0·0256	−0·0046	0·0261	−0·0036
− 3·4	0·0213	−0·0046	0·0218	−0·0038	0·0221	−0·0030
− 3·6	0·0182	−0·0038	0·0185	−0·0031	0·0188	−0·0024
− 3·8	0·0158	−0·0031	0·0160	−0·0025	0·0162	−0·0019
− 4·0	0·0137	−0·0025	0·0139	−0·0021	0·0141	−0·0016
− 4·5	0·0099	−0·0017	0·0100	−0·0013	0·0101	−0·0010
− 5·0	0·0073	−0·0012	0·0074	−0·0010	0·0075	−0·0007
− 5·5	0·0055	−0·0009	0·0056	−0·0007	0·0056	−0·0005
− 6·0	0·0043	−0·0006	0·0044	−0·0005	0·0044	−0·0004
− 6·5	0·0034	−0·0005	0·0035	−0·0004	0·0035	−0·0003
− 7·0	0·0027	−0·0004	0·0028	−0·0003	0·0028	−0·0002
− 7·5	0·0022	−0·0003	0·0023	−0·0002	0·0023	−0·0002
− 8·0	0·0018	−0·0002	0·0018	−0·0002	0·0018	−0·0001
− 8·5	0·0015	−0·0002	0·0015	−0·0001	0·0015	−0·0001
− 9·0	0·0013	−0·0002	0·0013	−0·0001	0·0013	−0·0001
− 9·5	0·0011	−0·0001	0·0011	−0·0001	0·0011	−0·0000
−10·0	0·0010	−0·0001	0·0010	−0·0000	0·0010	−0·0000
$\frac{1}{\pi}\int_{x/\eta_{cyl}+10}^{\infty} \begin{matrix} u^* \\ v^* \end{matrix} d\frac{\xi}{\eta_{cyl}}$	0·0050	−0·0003	0·0050	−0·0002	0·0050	−0·0002

TABLE 2—*continued*

$\frac{x-\xi}{\eta_{cyl}}$	$\frac{y}{\eta_{cyl}} = 0{\cdot}20$		$\frac{y}{\eta_{cyl}} = 0{\cdot}10$		$\frac{y}{\eta_{cyl}} = 0{\cdot}00$	
	$\frac{1}{\pi}u^*$	$\frac{1}{\pi}v^*$	$\frac{1}{\pi}u^*$	$\frac{1}{\pi}v^*$	$\frac{1}{\pi}u^*$	$\frac{1}{\pi}v^*$
0	1·03	0	1·01	0	1·000	0
− 0·01	1·03	−0·0031	1·01	−0·0015	1·000	0
− 0·04	1·03	−0·0126	1·01	−0·0059	0·998	0
− 0·09	1·01	−0·0284	0·993	−0·0132	0·987	0
− 0·16	0·985	−0·0484	0·965	−0·0227	0·963	0
− 0·25	0·927	−0·0691	0·916	−0·0331	0·913	0
− 0·36	0·840	−0·0848	0·834	−0·0417	0·834	0
− 0·49	0·707	−0·0911	0·722	−0·0442	0·724	0
− 0·64	0·592	−0·0828	0·595	−0·0408	0·598	0
− 0·81	0·461	−0·0678	0·464	−0·0334	0·466	0
− 1·00	0·347	−0·0522	0·350	−0·0264	0·353	0
− 1·2	0·257	−0·0379	0·260	−0·0191	0·262	0
− 1·4	0·192	−0·0269	0·195	−0·0137	0·196	0
− 1·6	0·146	−0·0199	0·148	−0·0104	0·149	0
− 1·8	0·113	−0·0149	0·114	−0·0076	0·114	0
− 2·0	0·0882	−0·0110	0·0891	−0·0057	0·0894	0
− 2·2	0·0698	−0·0082	0·0703	−0·0042	0·0705	0
− 2·4	0·0560	−0·0061	0·0563	−0·0032	0·0565	0
− 2·6	0·0455	−0·0047	0·0457	−0·0024	0·0459	0
− 2·8	0·0376	−0·0037	0·0378	−0·0019	0·0379	0
− 3·0	0·0313	−0·0030	0·0315	−0·0015	0·0316	0
− 3·2	0·0264	−0·0025	0·0265	−0·0013	0·0265	0
− 3·4	0·0223	−0·0020	0·0224	−0·0011	0·0224	0
− 3·6	0·0190	−0·0017	0·0191	−0·0009	0·0191	0
− 3·8	0·0164	−0·0013	0·0164	−0·0007	0·0164	0
− 4·0	0·0142	−0·0011	0·0143	−0·0006	0·0143	0
− 4·5	0·0102	−0·0007	0·0102	−0·0004	0·0102	0
− 5·0	0·0075	−0·0005	0·0075	−0·0003	0·0075	0
− 5·5	0·0057	−0·0004	0·0057	−0·0002	0·0057	0
− 6·0	0·0044	−0·0003	0·0044	−0·0002	0·0044	0
− 6·5	0·0035	−0·0002	0·0035	−0·0001	0·0035	0
− 7·0	0·0028	−0·0001	0·0028	−0·0001	0·0028	0
− 7·5	0·0023	−0·0001	0·0023	−0·0001	0·0023	0
− 8·0	0·0018	−0·0001	0·0018	0·0000	0·0018	0
− 8·5	0·0015	−0·0001	0·0015	0·0000	0·0015	0
− 9·0	0·0013	0·0000	0·0013	0·0000	0·0013	0
− 9·5	0·0011	0·0000	0·0011	0·0000	0·0011	0
−10·0	0·0010	0·0000	0·0010	0·0000	0·0010	0
$\frac{1}{\pi}\int_{x/\eta_{cyl}+10}^{\infty} \begin{matrix} u^* \\ v^* \end{matrix} d\frac{\xi}{\eta_{cyl}}$	0·0050	−0·0001	0·0050	−0·0001	0·0050	0

TABLE 3

$(1/\pi)E(k^2)$

k^2	0	1	2	3	4	5	6	7	8	9	10	
0·0	0·500	0·499	0·497	0·496	0·495	0·494	0·492	0·491	0·490	0·489	0·487	0·9
0·1	0·487	0·486	0·485	0·483	0·482	0·481	0·479	0·478	0·477	0·475	0·474	0·8
0·2	0·474	0·473	0·471	0·470	0·469	0·467	0·466	0·464	0·463	0·462	0·460	0·7
0·3	0·460	0·459	0·457	0·456	0·454	0·453	0·451	0·450	0·449	0·447	0·445	0·6
0·4	0·445	0·444	0·442	0·441	0·439	0·438	0·436	0·435	0·433	0·432	0·430	0·5
0·5	0·430	0·428	0·427	0·425	0·423	0·422	0·420	0·418	0·417	0·415	0·413	0·4
0·6	0·413	0·412	0·410	0·408	0·406	0·405	0·403	0·401	0·399	0·397	0·395	0·3
0·7	0·395	0·393	0·391	0·389	0·388	0·386	0·384	0·381	0·379	0·377	0·375	0·2
0·8	0·375	0·373	0·371	0·369	0·366	0·364	0·362	0·359	0·357	0·354	0·352	0·1
0·9	0·352	0·349	0·346	0·344	0·341	0·338	0·334	0·331	0·327	0·323	0·318	0·0
	10	9	8	7	6	5	4	3	2	1	0	k'^2

TABLE 4

$(1/\pi)\,[K(k^2) - E(k^2)]$

k^2	0	1	2	3	4	5	6	7	8	9	10	
0·0	0	0·00251	0·00504	0·00758	0·0102	0·0128	0·0153	0·0179	0·0206	0·0233	0·0260	0·9
0·1	0·0260	0·0287	0·0315	0·0342	0·0370	0·0398	0·0426	0·0456	0·0485	0·0514	0·0544	0·8
0·2	0·0544	0·0574	0·0604	0·0634	0·0665	0·0695	0·0726	0·0758	0·0790	0·0823	0·0855	0·7
0·3	0·0855	0·0888	0·0922	0·0956	0·0989	0·102	0·106	0·110	0·113	0·117	0·120	0·6
0·4	0·120	0·124	0·128	0·132	0·136	0·140	0·144	0·148	0·152	0·156	0·160	0·5
0·5	0·160	0·165	0·169	0·174	0·178	0·183	0·187	0·192	0·197	0·202	0·207	0·4
0·6	0·207	0·213	0·218	0·223	0·229	0·235	0·241	0·246	0·253	0·259	0·265	0·3
0·7	0·265	0·272	0·279	0·286	0·293	0·301	0·309	0·317	0·325	0·334	0·343	0·2
0·8	0·343	0·353	0·363	0·374	0·385	0·397	0·409	0·422	0·437	0·452	0·469	0·1
0·9	0·469	0·488	0·508	0·531	0·557	0·588	0·626	0·674	0·740	0·853	∞	0·0
	10	9	8	7	6	5	4	3	2	1	0	k'^2

TABLE 4a

$(1/\pi)\,[K(k^2) - E(k^2)]$ *for* $k^2 \approx 1$ *in function of* $k'^2 = 1 - k^2$

k'^2	$\times 10^{-(8+n)}$	$\times 10^{-7}$	$\times 10^{-6}$	$\times 10^{-5}$	$\times 10^{-4}$	$\times 10^{-3}$
1	$3{\cdot}06 + 0{\cdot}37n$	2·69	2·32	1·96	1·59	1·22
2	$2{\cdot}95 + 0{\cdot}37n$	2·58	2·21	1·85	1·48	1·11
3	$2{\cdot}88 + 0{\cdot}37n$	2·51	2·15	1·78	1·41	1·05
4	$2{\cdot}84 + 0{\cdot}37n$	2·47	2·10	1·74	1·37	1·00
5	$2{\cdot}80 + 0{\cdot}37n$	2·43	2·07	1·70	1·33	0·965
6	$2{\cdot}77 + 0{\cdot}37n$	2·40	2·04	1·67	1·30	0·935
7	$2{\cdot}75 + 0{\cdot}37n$	2·38	2·01	1·65	1·28	0·911
8	$2{\cdot}73 + 0{\cdot}37n$	2·36	1·99	1·62	1·26	0·889
9	$2{\cdot}71 + 0{\cdot}37n$	2·34	1·97	1·61	1·24	0·870
10	$2{\cdot}69 + 0{\cdot}37n$	2·32	1·96	1·59	1·22	0·853

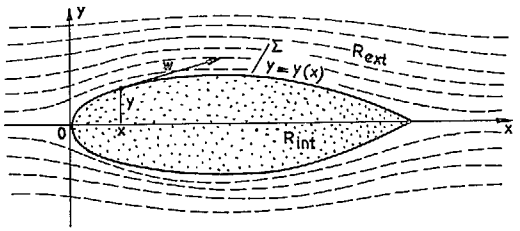

FIG. 1. Generation of a symmetrical body by a vortex layer on its surface.

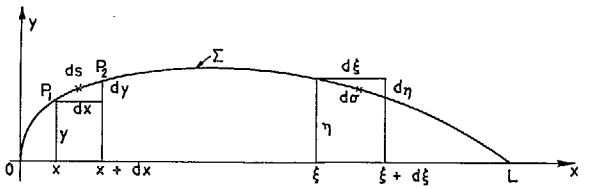

FIG. 3. Notation.

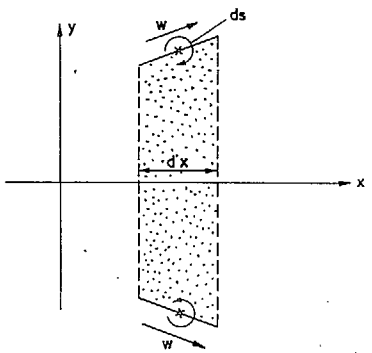

FIG. 2. The strength of the generating vortex layer per unit length of arc equals the velocity at the surface.

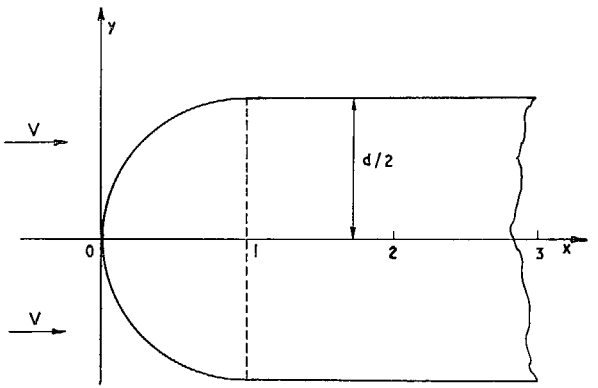

FIG. 4. Numerical example for the two-dimensional case: semi-infinite plate with a semi-circular leading edge.

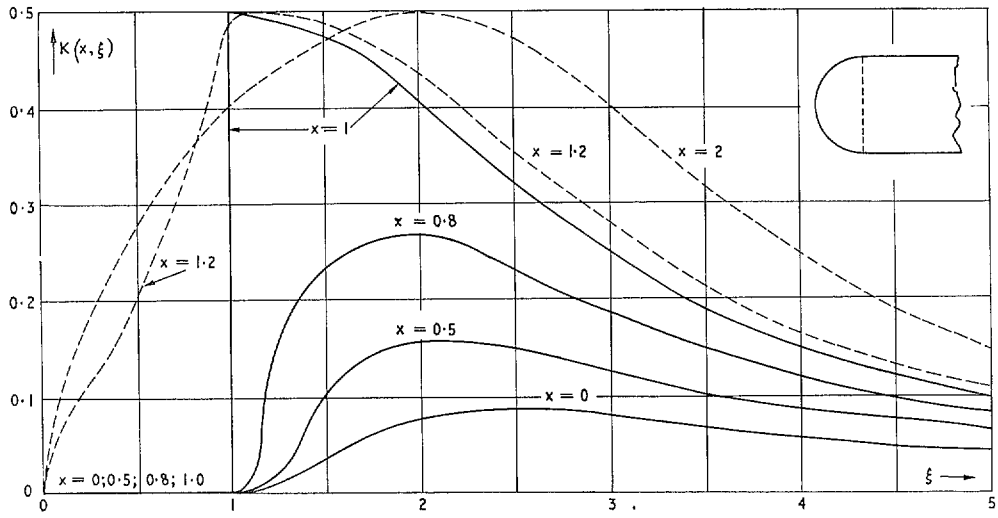

FIG. 5. Semi-infinite plate with a semi-circular leading edge: kernel of the integral equation.

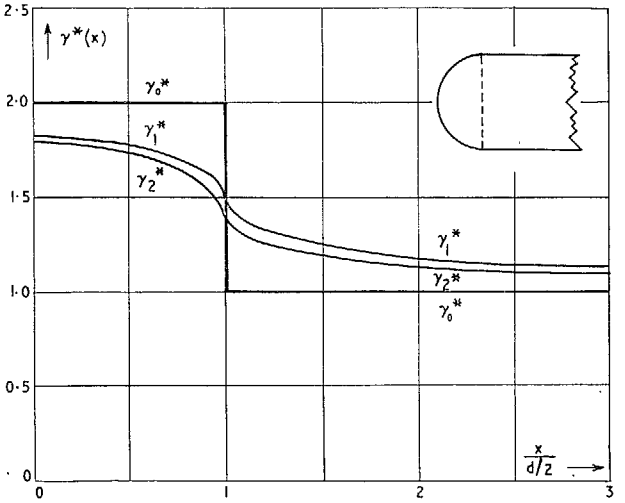

FIG. 6. Semi-infinite plate with a semi-circular leading edge; solution $\gamma^*(x)$ of the integral equation.

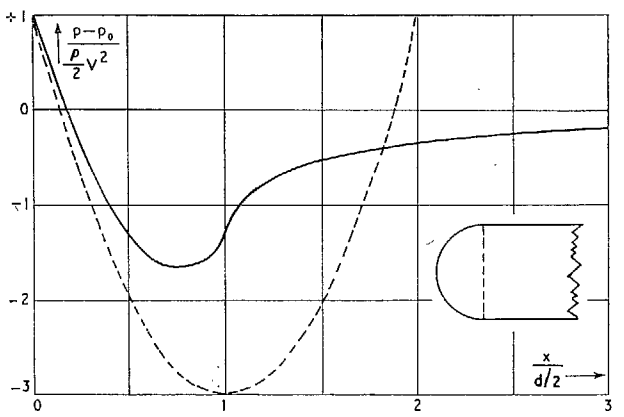

FIG. 7. Semi-infinite plate with a semi-circular leading edge: pressure distribution, calculated from γ_2^*. For comparison, the pressure distribution of a circular cylinder (dotted line).

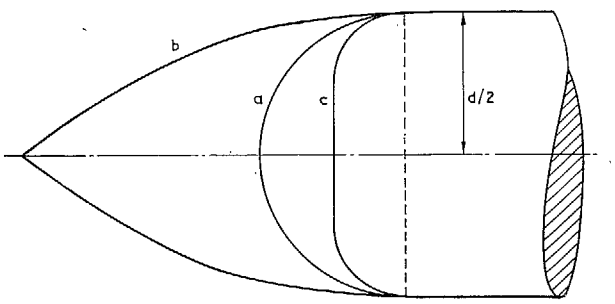

FIG. 8. Numerical examples for the three-dimensional case: semi-infinite cylinder with three different heads (hemispherical, 2 caliber ogival and $\frac{1}{4}$ caliber rounded).

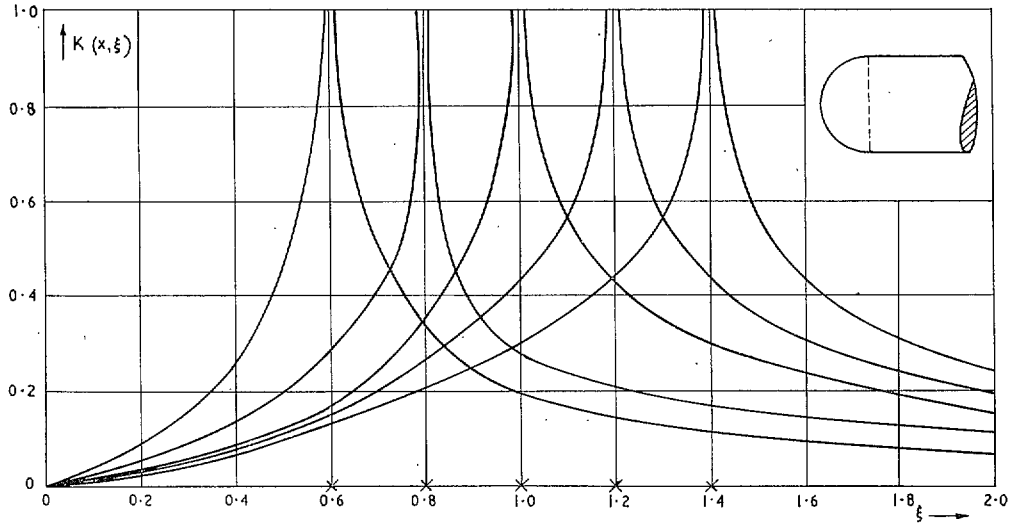

FIG. 9. Kernel of the integral equation for a semi-infinite cylinder with a hemispherical head. Pivotal points $x = 0{\cdot}6, 0{\cdot}8, 1, 1{\cdot}2, 1{\cdot}4$.

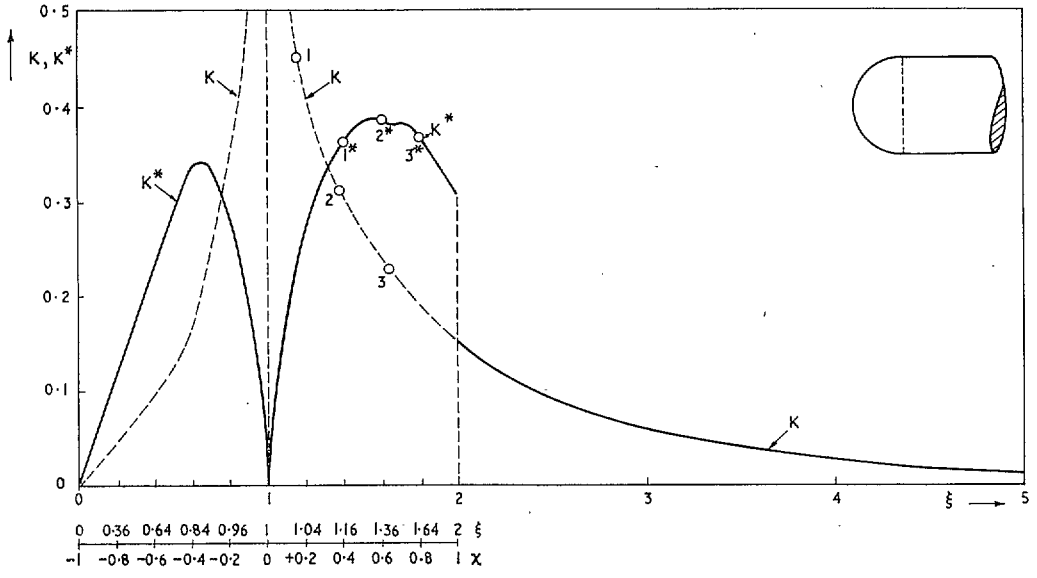

FIG. 10. Semi-infinite cylinder with a hemispherical head. Kernel K and transformed kernel K^* for $x = 1{\cdot}0$. (1, 1*, etc. are corresponding points in the transformation.)

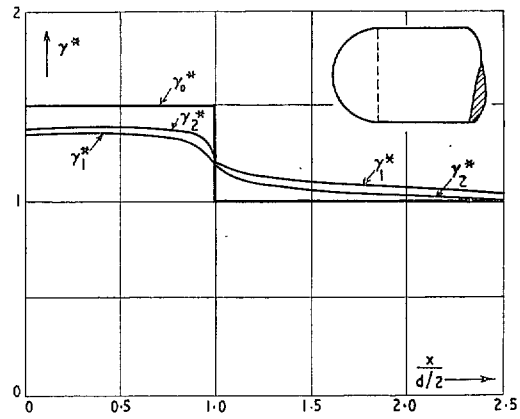

FIG. 11. Semi-infinite cylinder with a hemispherical head. Solution $\gamma^*(x)$ of the integral equation.

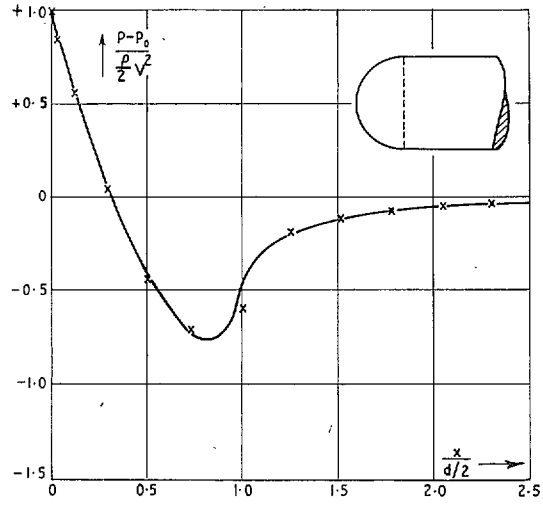

FIG. 12. Semi-infinite cylinder with a hemispherical head. Pressure distribution. Theoretical curve and experimental results. ($Re = 2 \times 10^5$, Ref. 13a.)

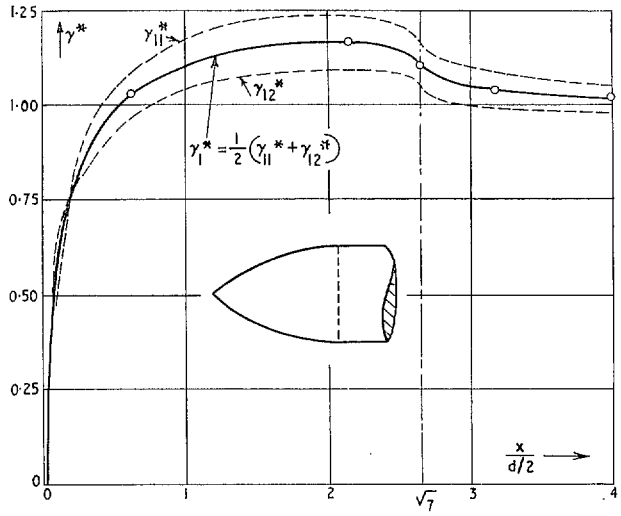

FIG. 13. Semi-infinite cylinder with a 2 caliber ogival head. Solution $\gamma^*(x)$ of the integral equation. Circles = points of the second approximation $\gamma_{21}{}^*(x)$.

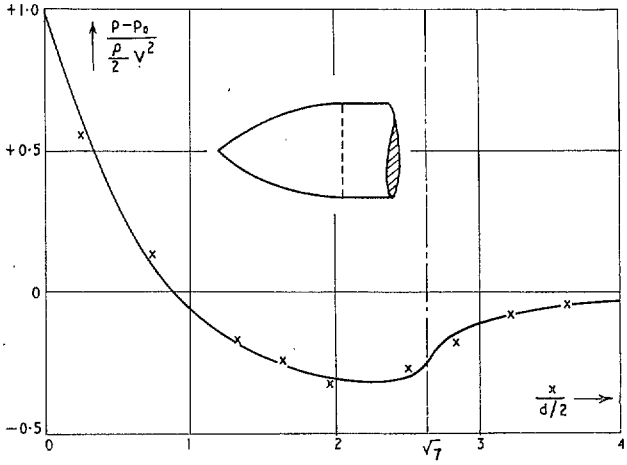

FIG. 14. Semi-infinite cylinder with a 2 caliber ogival head. Pressure distribution, theoretical and experimental. ($Re = 2 \times 10^5$.)

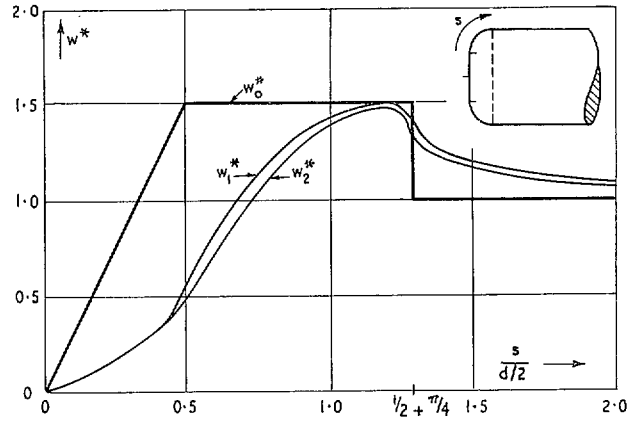

FIG. 15. Semi-infinite cylinder with a $\frac{1}{4}$ caliber rounded head. Velocity distribution as function of the length of arc. (Solution of the integral equation.)

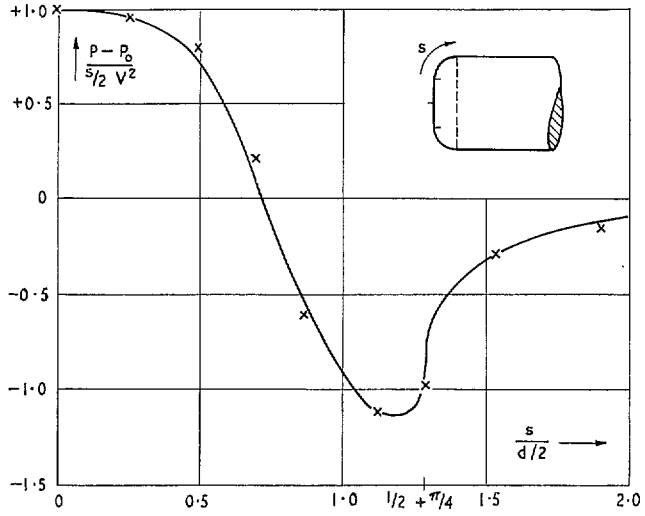

FIG. 16. Semi-infinite cylinder with a $\frac{1}{4}$ caliber rounded head. Pressure distribution as function of the length of arc, theoretical and experimental. ($Re = 2 \times 10^5$.)

(89800) Wt. 65/1418 K.5 8/64 Hw.

Publications of the Aeronautical Research Council

ANNUAL TECHNICAL REPORTS OF THE AERONAUTICAL RESEARCH COUNCIL (BOUND VOLUMES)

1942 Vol. I. Aero and Hydrodynamics, Aerofoils, Airscrews, Engines. 75*s.* (post 2*s.* 9*d.*)
Vol. II. Noise, Parachutes, Stability and Control, Structures, Vibration, Wind Tunnels. 47*s.* 6*d.* (post 2*s.* 3*d.*)

1943 Vol. I. Aerodynamics, Aerofoils, Airscrews. 80*s.* (post 2*s.* 6*d.*)
Vol. II. Engines, Flutter, Materials, Parachutes, Performance, Stability and Control, Structures. 90*s.* (post 2*s.* 9*d.*)

1944 Vol. I. Aero and Hydrodynamics, Aerofoils, Aircraft, Airscrews, Controls. 84*s.* (post 3*s.*)
Vol. II. Flutter and Vibration, Materials, Miscellaneous, Navigation, Parachutes, Performance, Plates and Panels, Stability, Structures, Test Equipment, Wind Tunnels. 84*s.* (post 3*s.*)

1945 Vol. I. Aero and Hydrodynamics, Aerofoils. 130*s.* (post 3*s.* 6*d.*)
Vol. II. Aircraft, Airscrews, Controls. 130*s.* (post 3*s.* 6*d.*)
Vol. III. Flutter and Vibration, Instruments, Miscellaneous, Parachutes, Plates and Panels, Propulsion. 130*s.* (post 3*s.* 3*d.*)
Vol. IV. Stability, Structures, Wind Tunnels, Wind Tunnel Technique. 130*s.* (post 3*s.* 3*d.*)

1946 Vol. I. Accidents, Aerodynamics, Aerofoils and Hydrofoils. 168*s.* (post 3*s.* 9*d.*)
Vol. II. Airscrews, Cabin Cooling, Chemical Hazards, Controls, Flames, Flutter, Helicopters, Instruments and Instrumentation, Interference, Jets, Miscellaneous, Parachutes. 168*s.* (post 3*s.* 3*d.*)
Vol. III. Performance, Propulsion, Seaplanes, Stability, Structures, Wind Tunnels. 168*s.* (post 3*s.* 6*d.*)

1947 Vol. I. Aerodynamics, Aerofoils, Aircraft. 168*s.* (post 3*s.* 9*d.*)
Vol. II. Airscrews and Rotors, Controls, Flutter, Materials, Miscellaneous, Parachutes, Propulsion, Seaplanes, Stability, Structures, Take-off and Landing. 168*s.* (post 3*s.* 9*d.*)

1948 Vol. I. Aerodynamics, Aerofoils, Aircraft, Airscrews, Controls, Flutter and Vibration, Helicopters, Instruments, Propulsion, Seaplane, Stability, Structures, Wind Tunnels. 130*s.* (post 3*s.* 3*d.*)
Vol. II. Aerodynamics, Aerofoils, Aircraft, Airscrews, Controls, Flutter and Vibration, Helicopters, Instruments, Propulsion, Seaplane, Stability, Structures, Wind Tunnels. 110*s.* (post 3*s.* 3*d.*)

Special Volumes

Vol. I. Aero and Hydrodynamics, Aerofoils, Controls, Flutter, Kites, Parachutes, Performance, Propulsion, Stability. 126*s.* (post 3*s.*)
Vol. II. Aero and Hydrodynamics, Aerofoils, Airscrews, Controls, Flutter, Materials, Miscellaneous, Parachutes, Propulsion, Stability, Structures. 147*s.* (post 3*s.*)
Vol. III. Aero and Hydrodynamics, Aerofoils, Airscrews, Controls, Flutter, Kites, Miscellaneous, Parachutes, Propulsion, Seaplanes, Stability, Structures, Test Equipment. 189*s.* (post 3*s.* 9*d.*)

Reviews of the Aeronautical Research Council

1939–48 3*s.* (post 6*d.*) 1949–54 5*s.* (post 5*d.*)

Index to all Reports and Memoranda published in the Annual Technical Reports

1909–1947 R. & M. 2600 (out of print)

Indexes to the Reports and Memoranda of the Aeronautical Research Council

Between Nos. 2351–2449	R. & M. No. 2450	2*s.* (post 3*d.*)
Between Nos. 2451–2549	R. & M. No. 2550	2*s.* 6*d.* (post 3*d.*)
Between Nos. 2551–2649	R. & M. No. 2650	2*s.* 6*d.* (post 3*d.*)
Between Nos. 2651–2749	R. & M. No. 2750	2*s.* 6*d.* (post 3*d.*)
Between Nos. 2751–2849	R. & M. No. 2850	2*s.* 6*d.* (post 3*d.*)
Between Nos. 2851–2949	R. & M. No. 2950	3*s.* (post 3*d.*)
Between Nos. 2951–3049	R. & M. No. 3050	3*s.* 6*d.* (post 3*d.*)
Between Nos. 3051–3149	R. & M. No. 3150	3*s.* 6*d.* (post 3*d.*)

HER MAJESTY'S STATIONERY OFFICE

from the addresses overleaf

Printed and published by
HER MAJESTY'S STATIONERY OFFICE

To be purchased from
York House, Kingsway, London W.C.2
423 Oxford Street, London W.1
13A Castle Street, Edinburgh 2
109 St. Mary Street, Cardiff
39 King Street, Manchester 2
50 Fairfax Street, Bristol 1
35 Smallbrook, Ringway, Birmingham 5
80 Chichester Street, Belfast 1
or through any bookseller

Printed in England

S.O. Code No. 23-3374